PHYSICAL REVIEW D VOLUME 16, NUMBER 5 1 SEPTEMBER 1977

Estimates of production cross sections and distributions for W bosons and hadronic jets in high-energy pp and $\bar{p}p$ collisions*

Ronald F. Peierls, T. L. Trueman, and Ling-Lie Wang
Brookhaven National Laboratory, Upton. New York 11973
(Received 13 April 1977)

Using the quark-parton model, with structure functions chosen to agree with electroproduction and lepton-pair-production data, the cross sections are calculated for the production of charged and neutral W mesons in high-energy pp collisions. The single- and double-particle distributions for the leptonic and hadronic decays of the W are presented along with leptonic background from electromagnetic pair production. Using the same model, the cross sections for production of single and double hadronic jets are also calculated using both colored-vector-gluon exchange and the Field-Feynman models for the elementary quark-quark scattering. It is concluded that the leptonic decay of the W should be a strong signal well above background, and that the parity violation of the weak interaction leads to characteristically different distributions for leptons and antileptons. The production in proton-antiproton collisions is also studied and found to be only slightly above the proton-proton production. The cross section does not increase rapidly with energy for $s/m_W{}^2 \gtrsim 10$. For hadronic jet production, the vector-gluon and Field-Feynman models lead to significantly different distributions, and if the predictions of the former are true the hadronic jet decay of the W, although plentiful, will be difficult to see above background. The effects of transverse motion of the W, neglected in the quark model, are found to be unimportant.

I. INTRODUCTION

Ever since the original theory of Yukawa, the mediating particles for weak interactions, the intermediate bosons W, have been expected to exist.[1] So far they have escaped observation. It may well be that intermediate bosons are too heavy for existing accelerators to produce. The similarities between the structure of weak interactions and electromagnetic interactions have led[2] to the suggestion that the appropriate scale for the mass of the W is $(\alpha/G)^{1/2} \approx 30$ GeV/c,[2] where α is the fine-structure constant and G is the Fermi coupling constant. In particular, the unified gauge theory of Weinberg and Salam,[3] whose successful predictions include the existence of the weak neutral current,[4] leads to a charged W mass of about 60 GeV/c^2 and a neutral W mass of about 75 GeV/c^2.[3-5] Given these masses, the intermediate bosons are energetically well within the reach of currently proposed pp and $p\bar{p}$ colliding/beam machines. Therefore it is important to give reliable estimates of the W production cross sections and to study the methods of observing them. There have been many such studies.[6,7] In view of the fact that in the past year there have been many new measurements of dilepton production in hadronic reactions, an updating of previous studies[8] is in order. This is one of the continuing efforts to update and refine the estimates of W production and the methods of observing them.

While this paper was in preparation we received other manuscripts bearing on some of the topics discussed here. Where they overlap with this work, we find, in general, qualitative agreement.[9,10]

One method to estimate the W production cross sections is to rely upon the principle of conserved vector current (CVC)[11] (i.e., the assumption that the charged weak current and the isovector part of the electromagnetic current form an isomultiplet) and the scaling hypothesis (i.e., the hypothesis that the dimensionless cross section $m^3 d\sigma/dm$ for electromagnetic production of a lepton pair in pp collisions is a function of s/m^2 alone, where m is the dilepton invariant mass and s is the pp invariant energy squared). Using CVC, and assuming the isoscalar part of the dilepton production to be small, the cross section for producing a W with mass m is approximately given by 0.1 GeV^{-2} times the corresponding $m^3 d\sigma/dm$ for dilepton production with m in GeV units.[6] If scaling in s/m^2 holds, the same cross sections can be used to predict cross sections for producing a heavier W at a correspondingly higher energy. Unfortunately such a procedure is still not possible. There are measurements of dilepton production cross sections for a wide range of energies and dilepton masses; however, they involve different experimental acceptances. Thus a direct comparison to check scaling is not yet possible. It is hoped that such an important study can be carried out in the near future.

Another approach is to use a quark-parton model, which specifically contains scaling and CVC.[12] In the model, the dilepton and W production cross sections are given in terms of the quark structure

functions in the hadrons. These structure functions are in principle determined from lepton-hadron inelastic scatterings. The coupling strength of the W to the quarks depends upon specific weak-interaction theories. The main uncertainty in this approach is that the antiquark distributions (in the proton) are not well determined in lepton-hadron inelastic scattering for $x \gtrsim 0.1$; here x is the fraction of the proton momentum carried by the quark. However, the dilepton production in pp reactions depends sensitively on the full distribution of the "sea" quarks, and therefore we have to determine the behavior of the sea-quark distribution from the dilepton production data.

Calculating according to each experimental acceptance, we compare the model calculation with the dilepton production data. To obtain fully integrated data for $m^3 d\sigma/dm$, we use the model to interpolate. In this way of studying the pp data a set of quark structure functions, which fit ep inelastic scattering as well as the $pp \to l\bar{l}+X$ cross section, is determined; then the $pp \to l\bar{l}+X$ data measured in different parts of phase space are interpolated to check scaling. We then use the quark structure functions to calculate various W production and decay product cross sections.

It is interesting to note that $\bar{p}p \to l\bar{l}+X$ reactions are dominated by valence-quark interactions in the region where the sea-quark distributions are uncertain. Therefore $p\bar{p} \to l\bar{l}+X$ reactions provide a definite check on the Drell-Yan model. It would be desirable to have such experiments in the future.

In Sec. II we present the current status of dilepton production experiments. Structure functions are obtained which adequately fit the data, while remaining consistent with the ep inelastic data. In contrast to the previous results of Ref. 8, the new data are consistent with the assumption of colored quarks and favor a steeper sea-quark distribution, such as $(1-x)^7$.

In Sec. III, using the quark structure functions of Sec. II, we calculate the $W^{\pm}$, W^0 production cross sections in pp and $\bar{p}p$ reactions and their distribution in longitudinal momentum $d\sigma/dx_F$, where $x_F = p_z^*/\frac{1}{2}\sqrt{s}$; p_z^* is the c.m. longitudinal momentum of the W.

In Sec. IV the momentum distributions are given for single and double leptons from W decays. Their characteristics, such as the location of the peaks and $V-A$ interference effects, are pointed out. Leptonic backgrounds from other sources are also given.

In Sec. V the production of hadrons and hadron jets via strong interactions is calculated in the quark-parton model. Two different models for the quark interactions are considered, one with $p_\perp^{-4}$ behavior for the invariant cross sections, the other with $p_\perp^{-8}$. Hadronic-jet decays of the W and the possibility for observing them are also discussed.

In Sec. VI the effects of W motion in the transverse direction are considered and found to be unimportant. Concluding remarks are contained in Sec. VII. Appendix A contains a general discussion of the formalism, while Appendix B gives the detailed formulas used for various calculations in this paper.

II. PRESENT STATUS OF LEPTON-PAIR PRODUCTION

Ideally, as stated in the Introduction, it would be best to check purely from experiment whether the dimensionless cross sections $m^3 d\sigma/dm$ are a function of s/m^2 alone. Since there are not enough data to do so, we shall compare the Drell-Yan model, which contains scaling, with the existing data. In the past year, the main bulk of the new data has been from Fermilab. These data are

(1) $pp \to \mu^+\mu^- + X$ at $E_{\rm lab} = 400$ GeV/c, $p_z^* \approx 0$, $5 \leq m_{\mu\bar{\mu}} \leq 9$ GeV/c^2, of Hom *et al.*,[13]

(2) $pp \to e^+e^- + X$ at $E_{\rm lab} = 400$ GeV/c, $p_z^* \approx 0$, $5 \leq m_{e\bar{e}} \leq 9$ GeV/c^2, of Hom *et al.*,[14]

(3) $np \to \mu^+\mu^- + X$ at $E_{\rm lab} = 300$ GeV/c, 400 GeV/c, $p_z^* \approx 0$ and $7 \leq m_{\mu\bar{\mu}} \leq 11$ GeV/c^2, of Kluberg *et al.*,[15]

(4) $np \to \mu^+\mu^- + X$ at $E_{\rm lab} = 300$ GeV/c, $p_z \geq 75$ GeV/c and $1.1 \leq m_{\mu\bar{\mu}} \leq 2.5$ GeV/c^2, of Binkley *et al.*,[16]

(4) $pp \to \mu^+\mu^- + X$ at $E_{\rm lab} = 225$ GeV/c, $0.05 \lesssim 2p_z^*/\sqrt{s} \lesssim 0.8$, and $1.5 \leq m_{\mu\bar{\mu}} \leq 2.7$ GeV/c^2, of Anderson *et al.*[17]

These experiments measured dilepton production over a wide range of dilepton mass. The energy variations are relatively limited. Therefore they cannot truly provide a check on scaling. The mass variation of the cross sections, however, depends crucially on the valence and the sea-quark distributions, and thus gives a better determination of the sea-quark distribution in the $x > 0.1$ region. Also, notice that these experiments have very different acceptances. A direct comparison of all of them is not possible. We compare these data first with the Drell-Yan model calculated according to the experimental acceptance.

In the Appendixes we give a simple presentation of the model and a list of formulas for virtual photon, virtual and real, intermediate boson production cross sections and their associated lepton momentum distributions. We find a set of quark structure functions that fit the ep inelastic scattering as well as give reasonable agreement with these dilepton production cross sections. We assume SU(3) color symmetry for the quarks, each

quark having with equal probability one of three colors.

The only valence quarks in the proton are up and down quarks. The "sea" contains in addition strange quarks and all three antiquarks (we assume a negligible amount of charmed quarks). All distributions of quarks in the sea are assumed to be identical. The distributions of the quarks thus obtained[18] are

$$s(x)=0.15(1-x)^7/x\,,$$
$$u(x)=1.79(1-x)^3(1+2.3x)/\sqrt{x}+s(x)\,, \tag{2.1}$$
$$d(x)=1.07(1-x)^{3.1}/\sqrt{x}+s(x)\,,$$

and

$$\bar{u}(x)=\bar{d}(x)=\bar{s}(x)=s(x)\,, \tag{2.2}$$

where s, u, and d stand for strange, up, and down quarks, respectively. For each particular color, these structure functions must be divided by 3.

In the Drell-Yan model the electromagnetic production cross section for lepton pairs from hadron collision is

$$m^3\frac{d\sigma}{dm dx_F}=\frac{8\pi\alpha^2}{3}\frac{F(\bar{x},\bar{x}')}{(x_F{}^2+4\tau)^{1/2}}\,, \tag{2.3}$$

where

$$\bar{x}\equiv\tfrac{1}{2}[(x_F{}^2+4\tau)^{1/2}+x_F]\,,$$
$$\bar{x}'\equiv\tfrac{1}{2}[(x_F{}^2+4\tau)^{1/2}-x_F]\,,$$
$$\tau\equiv m^2/s\,,$$
$$x_F\equiv p_z^*/\tfrac{1}{2}\sqrt{s}\,, \tag{2.4}$$

and

$$F(x,x')=\tfrac{1}{3}xx'\{\tfrac{4}{9}[u(x)\bar{u}(x')+\bar{u}(x)u(x')]$$
$$+\tfrac{1}{9}[d(x)\bar{d}(x')+\bar{d}(x)d(x')]$$
$$+\tfrac{1}{9}[s(x)\bar{s}(x')+s(x')\bar{s}(x)]\}\,,$$

where the factors $\frac{4}{9}$, $\frac{1}{9}$, and $\frac{1}{9}$ are the squared charges of the quarks in units of $(4\pi\alpha)^{1/2}$, and the factor $\frac{1}{3}$ comes from projecting color-singlet combinations.

To obtain the x_F-integrated data of $m^3d\sigma/dm$, so that we can put all the data together, we assume that the ratio of the data to the model calculation stays the same in the unobserved x_F region. The results are given in Fig. 1 with $m^3d\sigma/dm$ versus s/m^2. The main differences from the previous analysis of Ref. 7, which was mainly based upon the then-available BNL data,[19] are that the data are consistent with color SU(3) symmetry of the quarks and favor a sea-quark distribution which is steeper than $(1-x)^{3.5}$. In Fig. 2 we show an $m^3d\sigma/dm$ plot with three different sea-quark structure functions to give a comparison. In all our calculations we use the structure functions given by Eq. (2.1). The form $(1-x)^7$ is consistent with the quark-counting rules.[20]

Recently Lederman and Pope[21] carried out a new analysis of the old BNL experiments[19]

$$pU\to\mu^+\mu^-+X,\ \text{at}\ E_{\rm lab}=20.5,\ 25,\ 22\ \text{GeV}/c\,,$$
$$p_z\geq 12\ \text{GeV}/c\ \text{and}\ 1.5\ \text{GeV}/c\leq m_{\mu\bar{\mu}}\leq 5\ \text{GeV}/c\,.$$

Rather than dividing by a factor of $235^{0.6}$ to obtain $pp\to\mu^+\mu^-+X$ cross sections, they divided by $235^{0.8}$ in the small-mass region, gradually increasing to 235 in the large-mass region. Using the same procedure for these newly analyzed data we present these points in sectioned open circles in Fig. 1. We see that this new interpretation of the BNL data brings their data into agreement

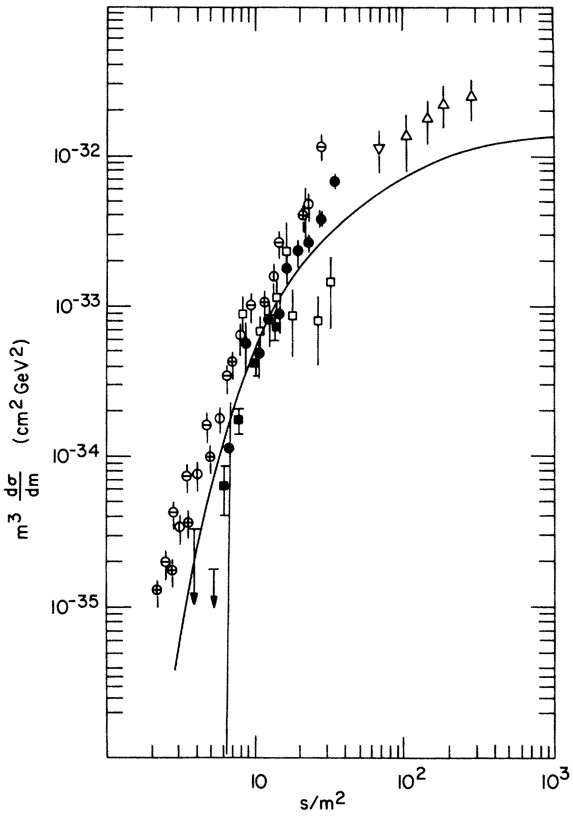

FIG. 1. $m^3d\sigma/dm$ vs s/m^2 for $pp\to l^+l^-+X$, where m is the lepton-pair invariant mass. The solid line is the Drell-Yan-model calculation using the quark structure functions given in Eq. (2.2). The data points are from experiments interpolated according to the model as described in the text. ●: $pp\to\mu^+\mu^-+X$ at $E_{\rm lab}=400$ GeV/c, Hom *et al.*, Ref. 13. □: $pp\to e^+e^-+X$ at $E_{\rm lab}=400$ GeV/c, Hom *et al.*, Ref. 14. ■: $np\to\mu^+\mu^-+X$ at $E_{\rm lab}=400$ GeV/c, Kluberg *et al.*, Ref. 15. △: $np\to\mu^+\mu^-+X$ at $E_{\rm lab}=300$ GeV/c, Binklet *et al.*, Ref. 16. ▽: $pp\to\mu^+\mu^-+X$ at $E_{\rm lab}=225$ GeV/c, Anderson *et al.*, Ref. 17. ⊕, ⊙, ⊖: $pp\to\mu^+\mu^-+X$ at $E_{\rm lab}=22$, 25, 29.5 GeV, respectively, Pope and Lederman, Ref. 21.

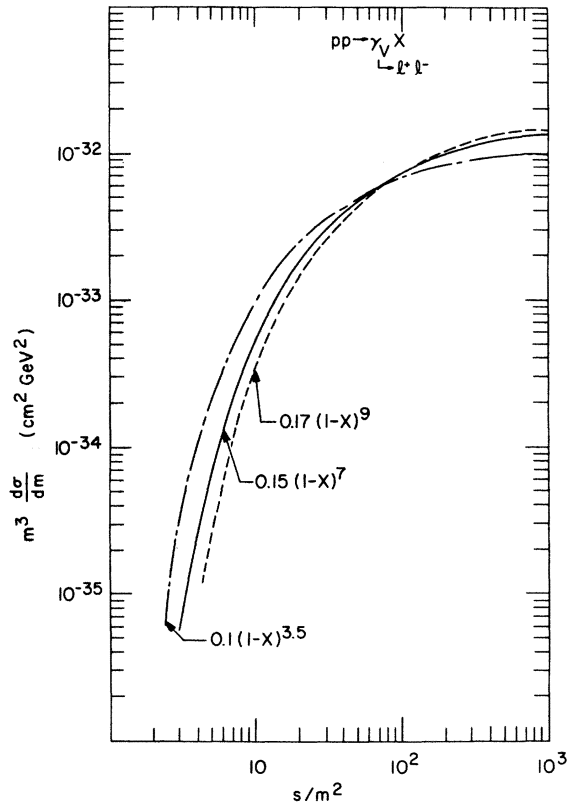

FIG. 2. $m^3 d\sigma/dm^2$ vs s/m^2 for $pp \to l^+ l^- X$ from the Drell-Yan model for three different choices of the sea-quark distribution $xs(x)$.

with the Fermilab data. Lederman and Pope have suggested that scaling is already observed. As cautious observers, we anxiously wait for the CERN ISR experiments, which are in progress, to give a more decisive verdict on scaling.

As noted previously, there is an uncertainty in the link between the dilepton production in pp reactions and the ep inelastic scattering via the Drell-Yan model, because lepton inelastic scattering is not sensitive to the sea-quark distribution for $x > 0.1$. Such an uncertainty is not there for the $p\bar{p}$ interaction, because there the valence quarks are in control. Therefore to check the Drell-Yan model more directly, it is important to do $p\bar{p} \to l\bar{l} + X$ experiments.

III. THE W PRODUCTION CROSS SECTIONS

As stated in the Introduction, once we obtain the scaling function $m^3 d\sigma/dm$ for electromagnetic production of lepton pairs, using CVC and assuming the isoscalar component of the virtual photon to be small, the W production cross section is estimated to be[6]

$$\sigma^W \approx \frac{3}{4}\frac{G/\sqrt{2}}{\alpha^2} m^3 \frac{d\sigma}{dm} \approx (0.1\ \text{GeV}^{-2}) \times m^3 \frac{d\sigma}{dm} . \quad (3.1)$$

Thus, if future experiments also confirm scaling, Fig. 1 already gives us a rough idea of the W production cross sections.

To be specific, we calculate the W production cross sections using the Drell-Yan model and the structure functions obtained in Sec. II and the formulas given in Appendix B. For the calculation of σ_W we use Eqs. (B12), (B13), and (B24). In Fig. 3 we give the production cross sections for $pp \to W^{\pm} X$, $p\bar{p} \to W^{\pm} X$ and in Fig. 4 we give the $pp \to W^0 X$ and $p\bar{p} \to W^0 X$ cross sections calculated according to the Weinberg-Salam model. Notice the following:

(1) In our calculation, $\sigma_{W^{\pm}}$ are truly scaling functions of s/m^2. The σ_{W^0} are calculated according to the Salam-Weinberg model [details are discussed in Appendix B, item (d)]. Owing to the fact that both the coupling strength and the mass of W^0 depend on the Weinberg angle θ_W, the σ_{W^0} are not scaling functions of s/m^2. The curve in Fig. 4, for $m_{W^0} = 77.5$ GeV/c corresponds to $\sin^2\theta_W \approx 0.4$ and varying s. We have also calculated σ_{W^0} for very different values of $\sin^2\theta_W$. As we can see from Eqs. (B19) and (B20) of Appendix B, the main

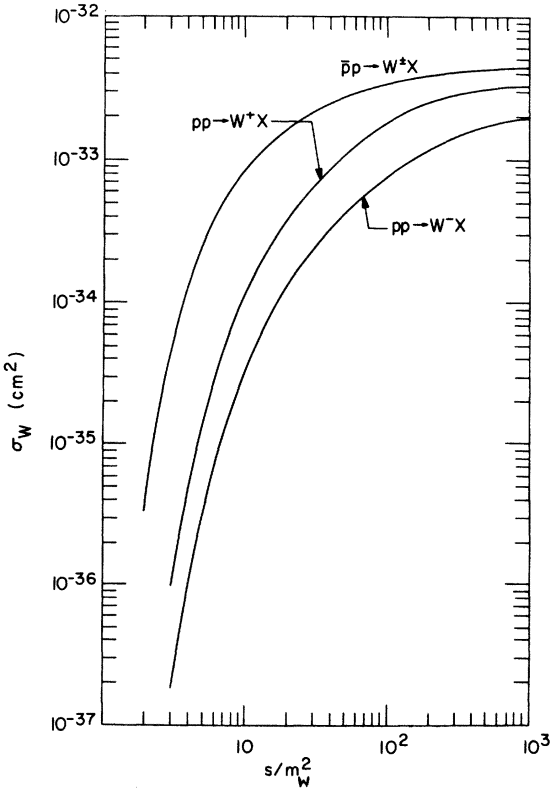

FIG. 3. $\sigma_{W^{\pm}}$ vs s/m_W^2 for $pp \to W^{\pm} X$ and $p\bar{p} \to W^{\pm} X$, calculated in the Drell-Yan model.

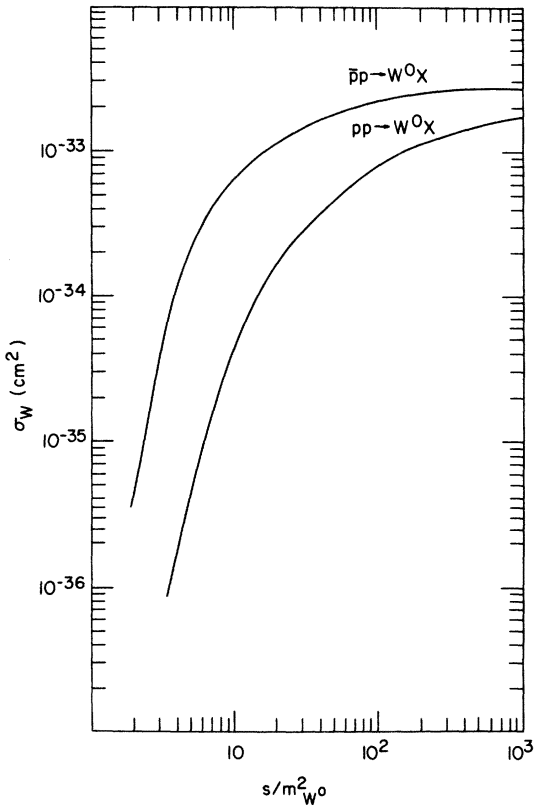

FIG. 4. σ_{W^0} vs $s/m_{W^0}{}^2$, with $m_{W^0} \approx 77.5$ GeV/c^2, $\sin^2\theta_W \approx 0.4$.

variations are in the W^0 mass and the vector coupling. It turns out that the σ_{W^0} plotted as a function of $s/m_{W^0}{}^2$ for various $\sin^2\theta_W$ are parallel curves differing by at most a factor of 3 or so. The value $\sin^2\theta_W \approx 0.4$, which is the currently favored value from neutrino experiments,[5] gives almost the smallest σ_{W^0} due to the smallness of the vector coupling to the up quark. We shall show later that this value of $\sin^2\theta_W$ also gives negligible parity-violation effects. $\sin^2\theta_W \approx 0.9$ gives the highest σ_{W^0}, about a factor three times the ones shown in Fig. 4.

(2) The cross sections σ_W rise sharply in the region $s/m^2 \lesssim 10$. This reflects the sharp rise of the quark and antiquark structure functions as x decreases from one. They then increase slowly as s/m^2 increases from 10. This reflects the fact that the ep inelastic function $\nu W_2(x)$ flattens off[22] as x decreases below 0.3. Once $s/m_W{}^2 \gtrsim 10$, not much is gained by going to higher energies. For a W mass up to 100 GeV/c an s value of $\approx 10^5$ (GeV)^2 will be adequate.

(3) The W production is significantly more abundant in the $p\bar{p}$ reaction than in pp for small s/m^2 $\lesssim 10$. This is due to the well-known property of quark-antiquark annihilation processes. In the small-s/m^2 region the valence-quark contribution is much larger than the sea-quark contribution. The W's are produced by valence-quark–valence-antiquark interactions in the $p\bar{p}$ reaction but by sea-antiquark–valence-quark interactions in the pp reaction. However, as s/m^2 increases the sea-quark contributions take over and the difference between the pp and $p\bar{p}$ reactions decreases. In view of the fact that the intensity of $\bar{p}$ beams are expected to be much lower than that of p beams, for sufficiently large s/m^2 ($\gtrsim 10$) a $\bar{p}p$ machine does not have any advantage for initial observation of the intermediate boson. However, there are interesting detailed features, which we shall discuss later, that make $\bar{p}p$ machines desirable for second-generation experiments.

In Fig. 5 we present $d\sigma_W/dx_F$, where $x_F = p_z^*/\frac{1}{2}\sqrt{s}$. Notice that most W's are produced in the small x_F region. As s/m^2 decreases, the x_F distribution broadens. A dip[23] (not zero) at $x_F = 0$ begins to show up for $s/m^2 \leq 3$. The dip is very mild and should have no effect on the search for W's in the small-x_F region.

IV. LEPTON DISTRIBUTIONS

As discussed in the preceding section, the production cross sections for the W's are rather

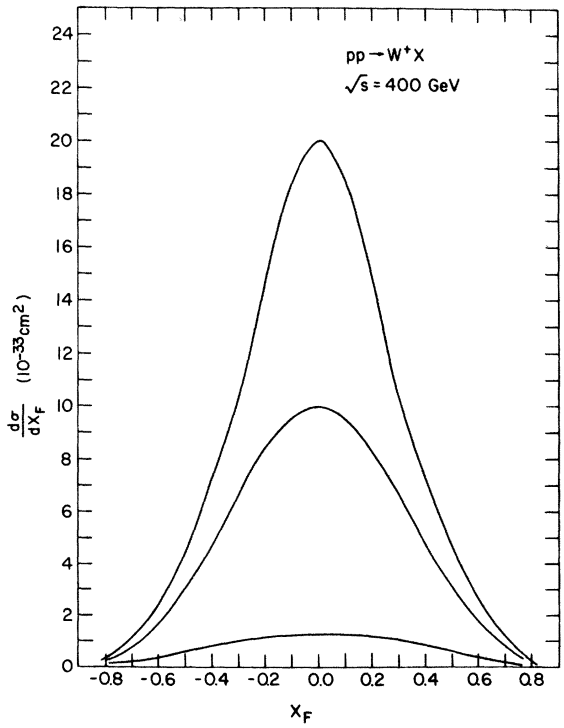

FIG. 5. $d\sigma/dx_F$ vs x_F for W^+, where $x_F \equiv 2p_z^*/\sqrt{s}$ for $s/m^2 = 70$, 35, and 10. The cross sections decrease with decreasing s/m^2.

large for $s/m_W^2 \gtrsim 10$. However, their detectability depends very much on the abundance of their decay products that are accessible to experimental detection. The W can either decay into a lepton pair or pure hadrons. We shall discuss the properties of hadronic decays in the next section. In this section we discuss the leptonic distributions from the W's and their background from electromagnetic production of leptons. Firstly we study the single-lepton distribution, which is the only observable particle from charged W's. Then we discuss the l^+l^- distributions from W^0.

A. Single-lepton distributions

The formulas for calculating various single-lepton distributions from $W^\pm$, W^0 in pp and $\bar{p}p$ reactions are given in Appendix B. Obviously there are very many distributions which could be plotted and discussed. In the following we shall discuss only the most distinctive features, using some representative W masses and energy ranges. Readers can extend these ideas to other particles and to different W masses and energies, and obtain some approximate estimates by looking at the figures in Sec. III, and the formulas in the Appendixes.

Among the important quantities are the W widths and branching ratios for leptonic decay. The leptonic width of the W can be calculated to be

$$\Gamma_{l\bar{l}} = \frac{1}{12\pi}\frac{G}{\sqrt{2}} m_W^3 . \tag{4.1}$$

To estimate its hadronic decay width we use the quark model of Glashow *et al.*,[24] in which the W^+ (W^-) couples with equal strength to the three colored $u\bar{d}$ ($\bar{u}d$) and the three colored $c\bar{s}$ ($\bar{c}s$) channels.[25] Adding these six channels to the two leptonic channels ($e\nu_e$, $\mu\nu_\mu$), we obtain the full width of the charged W's,

$$\Gamma_\pm = 8\,\frac{1}{12\pi}\frac{G}{\sqrt{2}} m_W^3 . \tag{4.2}$$

The leptonic branching ratio is $\frac{1}{8}$ for $e\nu_e$ or $\mu\nu_\mu$. So we see that the full width increases as the variety of quarks increases while the leptonic branching ratio decreases. Considering the fact that charmed particles[26] have already been found, and that three colors are reasonably consistent with existing experiment, Eq. (4.2) probably is an underestimate of the W width, but in the absence of any better guidance, we use it in our calculations. The estimates for the W^0 width are different, since the W^0 couples with different strength to different quark-antiquark pairs. We give the W^0 widths and its leptonic branching ratio in Appendix B. Equations (B21) and (B22) are calculated in the SU(2)⊗U(1) model of Weinberg and Salam[3] and Glashow *et al.*[24]

In Fig. 6 we show the l^+ distribution $d\sigma/dpd\Omega\,|_{90^\circ}$ vs $p_\perp$ from W^+ for some representative masses at $\sqrt{s} = 400$ GeV. Notice that the peak is always located at $p_\perp = \frac{1}{2}m_W$. The spread on the $p_\perp > \frac{1}{2}m_W$ side reflects the W width, but the spread on the $p_\perp < \frac{1}{2}m_W$ side reflects the longitudinal motion of the W. The parton-quark model does not give any transverse motion to the W. Any such motion certainly will bring about some smearing of the peak. This will be discussed in Sec. VI.

The height of the peak decreases as the mass of the W^+ increases for fixed s. There are two reasons for the decrease: One is that as the value of s/m_W^2 decreases the W production cross section, σ_W, decreases as shown in Figs. 3 and 4. The other reason is associated with the increase of the width of the W as m_W increases [see Eq. (4.2) and Eq. (B9) in Appendix B] thus decreasing the height of the peak.

In the same figure, we have also estimated the l^+ coming from other sources. One source is virtual-photon production, which we calculated according to the Drell-Yan model using Eqs. (A15) and (B3). Another is from our estimates of large $p_\perp$ pion production discussed in the next section multiplied by 10^{-4}, which is the currently observed lepton-to-pion production ratio.[27] We see that the W signal is well above the background.

In Fig. 7 we show the l^+ distribution $d\sigma/dpd\Omega\,|_{\theta_+}$ from W^+ for various angles θ_+ vs $p_\perp$ of the l^+ where θ_+ is the angle of l^+ away from the beam direction. Notice that the peak still occurs at $p_\perp = \frac{1}{2}m_W$. The reason for this is clear from Eq. (A15) of Appendix

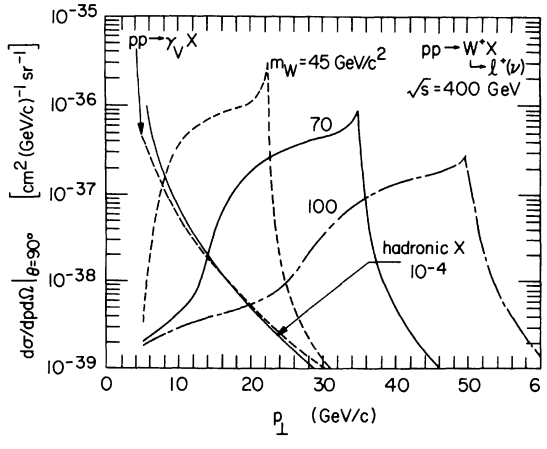

FIG. 6. $d\sigma/dpd\Omega\,|_{90^\circ}$ vs $p_\perp$ for an l^+ from W^+ with mass 45, 70, 100 GeV/c^2 at $\sqrt{s} = 400$ GeV, pp reaction. The smooth dashed curve is for l^+ from γ_V; the smooth solid curve is obtained by multiplying the pion distribution from vector gluons discussed in Sec. IV by 10^{-4}.

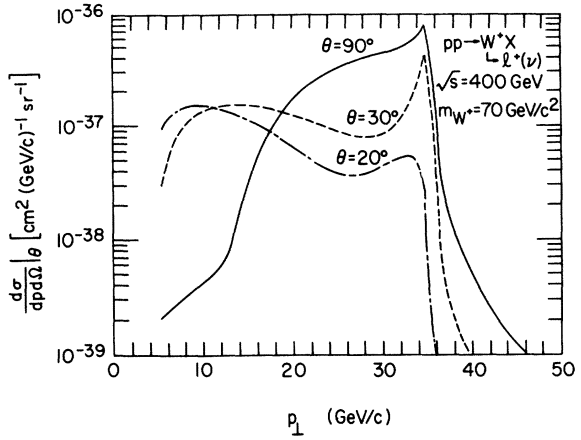

FIG. 7. $d\sigma/dpd\Omega$ vs $p_\perp$ for an l^+ from a W^+ with $m_W = 70$ GeV/c^2 at $\sqrt{s} = 400$ GeV, pp reaction, for $\theta = 90°$, 30°, 20°.

A. The longitudinal motion of the lepton arises from the compounding of the longitudinal motion of the W with the longitudinal motion in the W rest frame, i.e., its decay angular distribution. The decrease of the cross sections as θ_+ decreases reflects the decrease of W^+ production as its longitudinal momentum increases as shown in Fig. 5.

Further, owing to the vector–axial-vector mixed coupling of the W, l^+ and ν have very different longitudinal distributions in the W rest frame. The $V-A$ interaction projects out left-handed light fermions (such as l^-, ν, and quarks), and right-handed light antifermions (such as l^+, $\bar{\nu}$, and antiquarks). Owing to helicity conservation, l^-, ν (l^+, $\bar{\nu}$) are more likely to move in the direction of the quark (antiquark).

In the proton, the antiquarks give a narrower distribution in x_F than the quarks. Therefore we expect ν to have a wider distribution in longitudinal momentum than l^+. Since ν cannot be observed, we demonstrate this effect by comparing the longitudinal distributions of l^+ from W^+ and l^- from W^-.

In Fig. 8 we show $d\sigma/dpd\Omega$ vs θ for various values of $p_\perp$ of l^+ (l^-) from W^+ (W^-) with $m_W = 70$ GeV/c^2. We see that the $\cos\theta$ distribution for l^+ is rather flat and for l^- is very much forward and backward peaked. The former reflects the longitudinal distribution of the sea quarks and the latter reflects the longitudinal distribution of the valence quarks. Electromagnetically produced leptons would give identical distributions for l^+ and l^-.

The difference between the $l^\pm$ distributions shows up as soon as the weak interaction dominates the

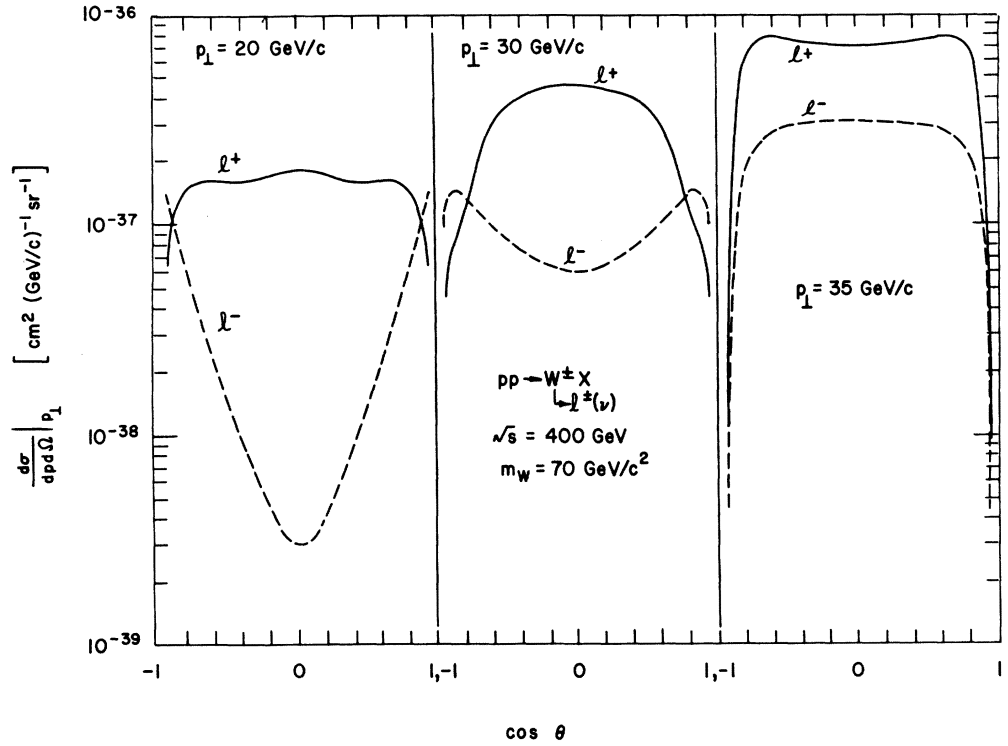

FIG. 8. $d\sigma/dpd\Omega$ vs θ for l^+ (solid curve) from W^+, and for l^- (dashed curve) from W^- with $m_{W^\pm} = 70$ GeV/c^2, $\sqrt{s} = 400$ GeV, pp reaction, for $p_\perp = 20$, 30, 35 GeV/c.

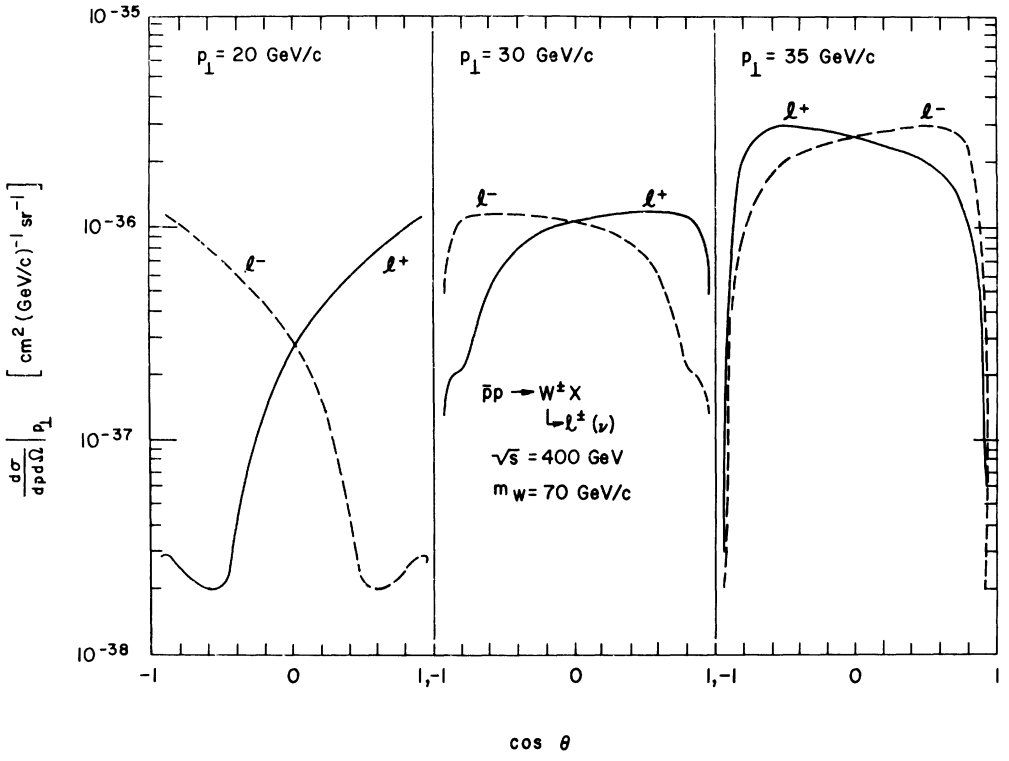

FIG. 9. Same as Fig. 8 for the $\bar{p}p$ reaction.

electromagnetic interaction, which happens at approximately $p_\perp = 15$ GeV/c for $m_W = 70$ GeV/c^2. The effect is enhanced as $p_\perp$ increases. However, as $p_\perp$ approaches $\frac{1}{2}m_W$, the effect disappears. The reason is that at $p_\perp = \frac{1}{2}m_W$, both l^+ and l^- have to move in the $p_\perp$ direction in the W rest frame. Thus the longitudinal motion of the leptons at $p_\perp = 35$ GeV/c in Fig. 8 comes completely from the $W^\pm$ longitudinal motion. The difference between the W^+ and W^- distributions reflects the difference between the distribution of up and down quarks.

The $V-A$ effect will show up even more dramatically in $\bar{p}p$ reactions. l^- and ν will tend to move in the proton direction and l^+, $\bar{\nu}$ will tend to move in the antiproton direction. In Fig. 9 we show such effects for $m_W = 70$ GeV/c^2 and $\sqrt{s} = 400$ GeV. It is interesting to note that the trend is reversed as the lepton $p_\perp$ reaches $\frac{1}{2}m_W = 35$ GeV/c^2. The reason is that at this value of $p_\perp$, the l^+ (l^-) distribution reflects completely the W^+ (W^-) longitudinal motion. The W^+ (W^-) tends to move in the proton (antiproton) direction owing to the dominance of the up quark (antiupquark) in the proton (antiproton). Thus we have this interesting switching of the forward-backward peaking of the l^+, l^- as $p_\perp$ approaches $\frac{1}{2}m_W$.

In Fig. 10 we show $d\sigma/dpd\Omega|_{\theta=90^\circ}$ vs $p_\perp$ for l^+ from weak interactions without W^+ (or an infinitely heavy W^+) compared to that from γ at $\sqrt{s} = 400$ GeV. We see that the weak interaction takes over from the electromagnetic interaction at $p_\perp \sim 25$ GeV/c. This is due to the fact that the electromagnetic interaction, though stronger in coupling strength, has a Q^{-4} propagator cutoff while the weak interaction in the region far below the intermediate-boson mass has none.

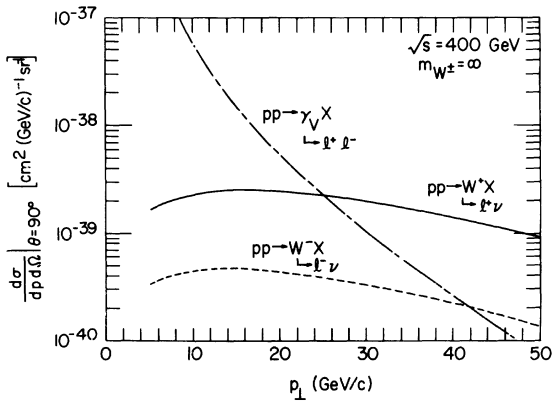

FIG. 10. $d\sigma/dpd\Omega|_{\theta=90^\circ}$ vs $p_\perp$ for an l^+ from weak interaction with an infinitely heavy W^+ (solid curve) and l^- from W^- (dashed curve) compared with that from γ_V (dot-dashed curve).

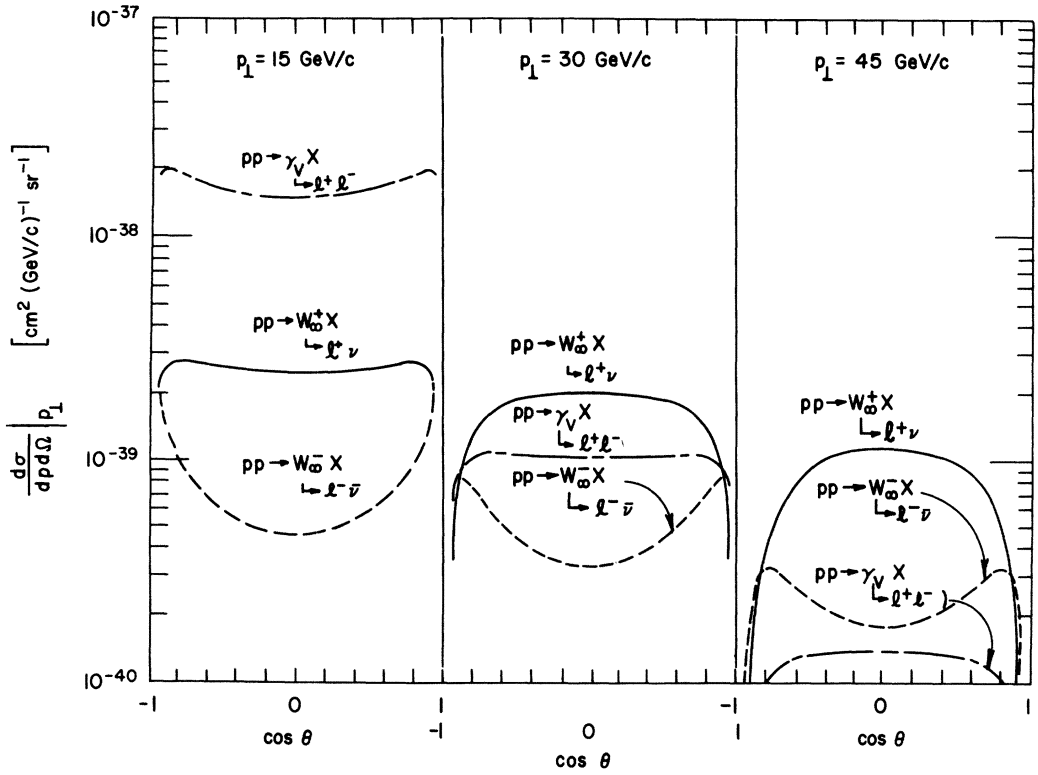

FIG. 11. Angular distributions of $l^\pm$ from $W^\pm$ of ∞ mass and from γ_V, for various values of $p_\perp$.

It is very hard to tell from Fig. 10 alone how to detect the onset of the weak interaction. Parity-nonconservation effects in the weak interaction as discussed previously will help to detect this crossover. In Fig. 11 we show the $\cos\theta$ distribution of l^+ and l^- from W_∞^+, γ_V, and W_∞^-, respectively, for three values of $p_\perp$. The l^+, l^- from γ_V, of course, have the same distributions.

For l^+, l^- from W^0, there is an additional term due to the interference between W^0 and γ_V (see the calculation at the end of Appendix B). In Fig. 12 we show $d\sigma/dpd\Omega|_{90^\circ}$ vs $p_\perp$ for l^+ from a W^0 of $m_{W^0} = 75$ GeV/c^2 at $\sqrt{s} = 400$ GeV for pp reaction.

As discussed previously and in detail at the end of Appendix B, the W^0 coupling to quarks and leptons is very model dependent. To illustrate this

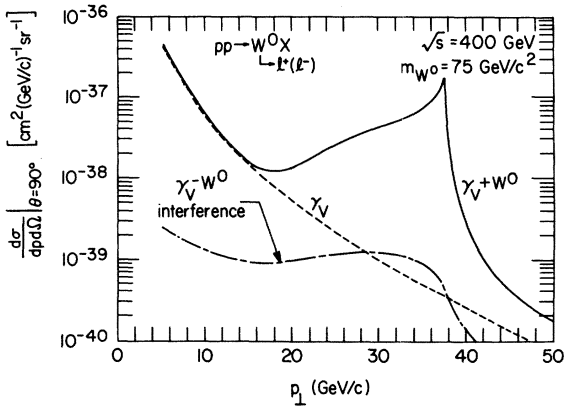

FIG. 12. $d\sigma/dpd\Omega|_{90^\circ}$ for l^+ from both W^0 and γ_V (solid curve) with $m_{W^0} \approx 75$ GeV/c^2 and $\sin^2\theta_W = 0.4$ at $\sqrt{s} = 400$ GeV (pp reaction). The dashed curve is from γ_V alone. The dash-dotted curve is from the interference of W^0 and γ_V.

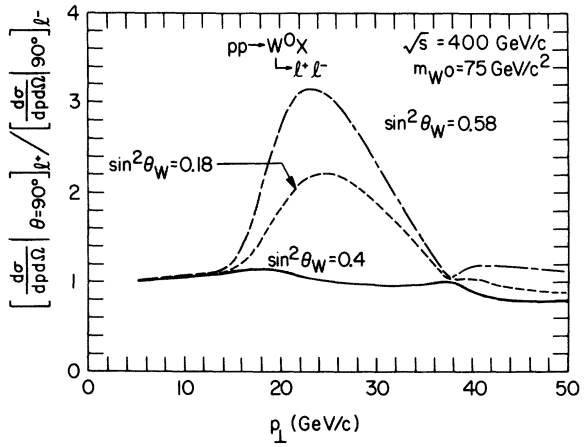

FIG. 13. The ratio of the l^+, l^- distributions $d\sigma/dpd\Omega|_{\theta=90^\circ}$ vs $p_\perp$ from W^0 and γ_V, with $m_{W^0} = 75$ GeV/c^2 at $\sqrt{s} = 400$ GeV (pp reaction, for various θ_W).

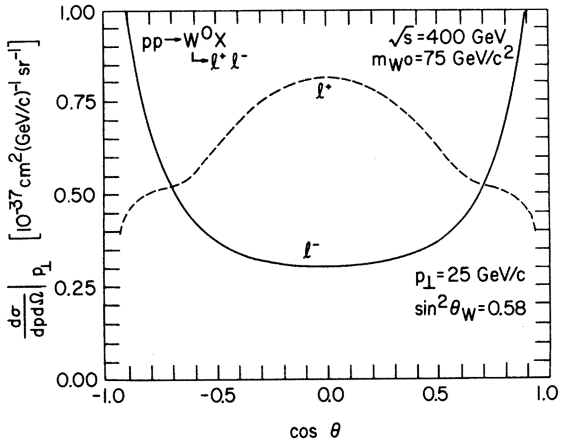

FIG. 14. $d\sigma/dp_\perp d\Omega|_{p_\perp=25\ \mathrm{GeV}/c}$ vs θ for l^+ (solid curve) and l^- (dotted curve) both from W^0 and γ_V, with $m_{W0} \approx 75\ \mathrm{GeV}/c^2$, $\sin^2\theta_W = 0.58$, and γ_V at $\sqrt{s} = 400$ GeV, pp reaction.

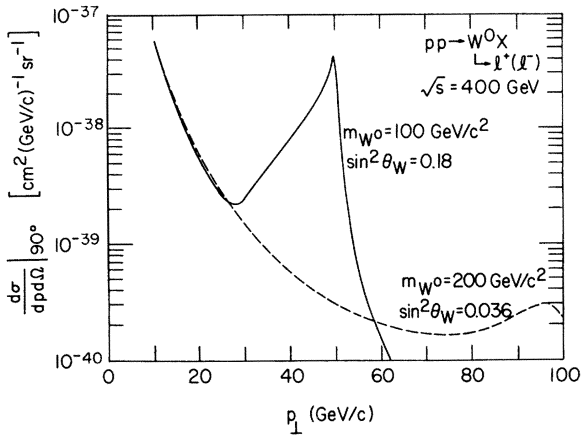

FIG. 16. $d\sigma/dpd\Omega|_{90^\circ}$ vs $p_\perp$ for l^+ from W^0 and γ_V at $\sqrt{s} = 400$ for $m_{W0} = 100\ \mathrm{GeV}/c^2$, $\sin^2\theta_W = 0.18$ (solid curve) and $m_{W0} = 200\ \mathrm{GeV}/c^2$, $\sin^2\theta_W = 0.036$ (dashed curve).

we show what happens when we modify the relation (B19) between mass and θ_W in the Weinberg-Salam model. In Fig. 13, we show the ratio of $(d\sigma/dp_+ d\Omega|_{\theta_+=90^\circ})(d\sigma/dp_- d\Omega|_{\theta=90^\circ})^{-1}$ vs $p_\perp$ for $\sin^2\theta_W = 0.4, 0.18, 0.58$ for fixed $m_{W0} = 75\ \mathrm{GeV}/c^2$ at $\sqrt{s} = 400\ \mathrm{GeV}$. We see that the experimentally preferred value $\sin^2\theta_W \approx 0.4$ gives a negligible difference between l^+ and l^-. This is because at $\sin^2\theta_W \approx 0.4$, the W coupling is predominantly axial [especially for the up quark, see Eq. (B20)]. For $\sin^2\theta_W$ away from 0.4, there are appreciable differences in the l^+, l^- distributions. At $\sin^2\theta_W = 1$, the interaction is maximally parity-violating and gives maximal difference in the l^+, l^- distributions. The ratio of l^+ to l^- distribution gets as high as 9 at $p_\perp = 25$ GeV/c. Note that in Fig. 13, the l^+ to l^- ratio always becomes unity at $p_\perp = \frac{1}{2}m_W = 37.5\ \mathrm{GeV}/c$. For $p_\perp = \frac{1}{2}m_W$ the longitudinal motions of l^+ and l^- are completely due to that of the W^0 and are therefore the same. In Fig. 14, we give $d\sigma/dpd\cos\theta|_{p_\perp}$ vs $\cos\theta$ with $p_\perp = 25\ \mathrm{GeV}/c$ for l^+ and l^- both from a W^0 with $m_{W0} = 75\ \mathrm{GeV}/c^2$, $\sqrt{s} = 400$ GeV. This demonstrates the full difference in the l^+, l^- longitudinal distributions. In Fig 15 we show the same plot as Fig. 14 but for $\bar{p}p$.

Returning to the Weinberg-Salam relation between mass and θ_W, in Fig. 16 we show $d\sigma/dpd\Omega|_{\theta=90^\circ}$ of l^+ from γ_V and W^0 for two values of $\sin^2\theta_W = 0.18$, 0.036 and the corresponding masses, $m_{W0} = 100$ and 200 GeV/c^2, respectively. The peak from the W^0 of 200 GeV/c^2 is barely above the γ_V background and would be difficult to observe. But in Fig. 17 the ratio of l^+ to l^- from $m_{W0} = 200\ \mathrm{GeV}/c^2$ is seen to be above 2 for a large range of $p_\perp$. Thus

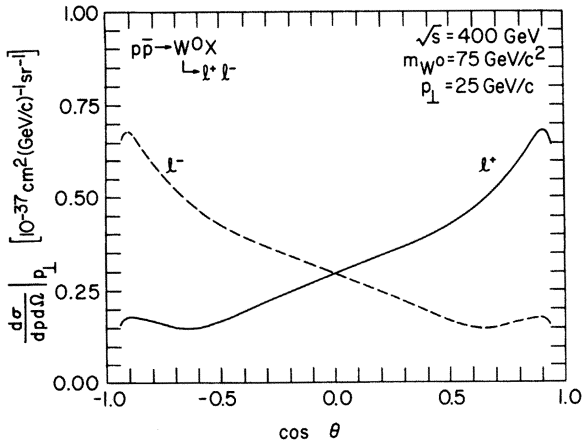

FIG. 15. Same as Fig. 14 for the $\bar{p}p$ reaction.

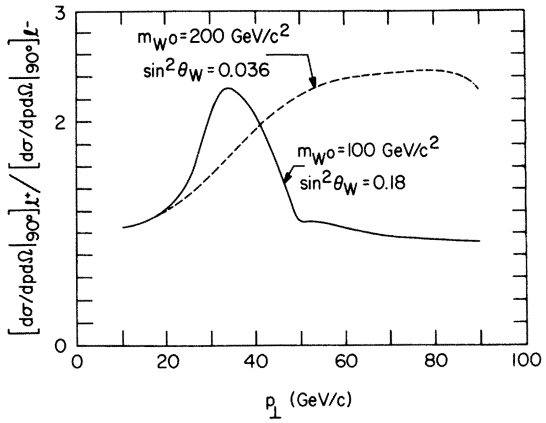

FIG. 17. The ratio of the l^+, l^- distributions $d\sigma/dpd\Omega|_{\theta=90^\circ}$ vs $p_\perp$ from W^0 and γ_V at $\sqrt{s} = 400$. The solid curve is for $m_{W0} = 100\ \mathrm{GeV}/c^2$, $\sin^2\theta_W = 0.18$, the dashed curve is for $m_{W0} = 200\ \mathrm{GeV}/c^2$, $\sin^2\theta_W = 0.036$.

a substantial V,A mixture provides a very important identification of the presence of weak-interaction effects. Of course, to ensure that both the measured $l^{\pm}$ come from a neutral W, the opposite charged lepton must also be detected in coincidence, though in general not at 90°.

B. Double-lepton distribution

The signal for W^0 is most obvious, i.e., a peak in the l^+l^- invariant mass. As mentioned earlier in Sec. III and in Appendix B, estimates for m_{W^0} and its coupling strength are very model dependent. However, we believe the characteristics presented in the following will be true whenever the W^0 effect manifests itself.

In Fig. 18 we show the invariant-mass distribution $d\sigma/dm_{l^+l^-}$ from W^0 and γ_V for an $m_{W^0}=75$ GeV/c^2 from $\sin^2\theta_W \approx 0.4$ at $\sqrt{s}=400$ GeV. Again we see that the W^0 signal is well above the background from γ_V.

In Fig. 19 we show the dependence on $p_{+\perp}$ for the distribution $d\sigma/dp_+d\Omega_+d\cos\theta_-|_{\theta_+=\theta_-=90^\circ}$ for l^+ and l^- coming from a W^0 of mass $m_{W^0}=75$ GeV/c^2 interfering with γ_V at $\sqrt{s}=400$ GeV.

In Fig. 20 we show the dependence on $\cos\theta_+$ of $(d\sigma/dp_+d\Omega_+d\cos\theta_-)_{\theta_-=90^\circ}$ with $p_{+\perp}=38.5$ GeV/c and 30 GeV/c for l^+,l^- from W^0 with $m_{W^0}=77$ GeV/c^2

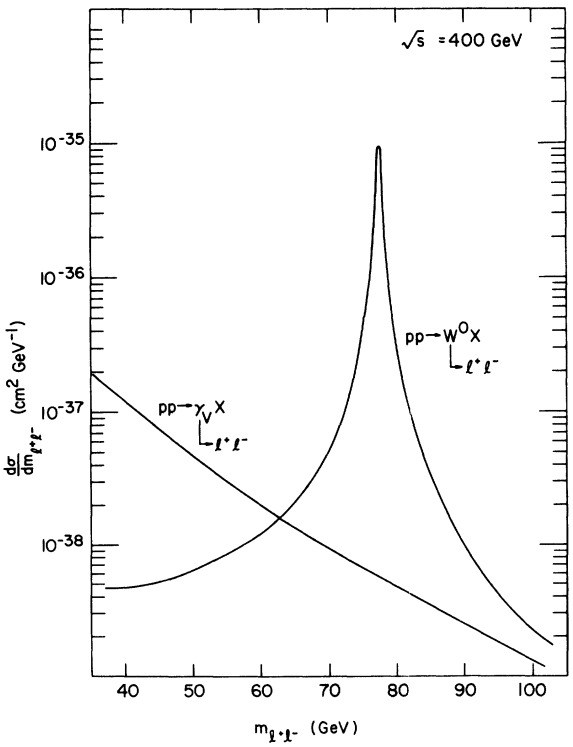

FIG. 18. $d\sigma/dm_{l^+l^-}$ for l^+,l^- from W^0 and γ_V with $m_{W^0} \approx 75$ GeV/c^2 at $\sqrt{s}=400$ GeV, pp reaction.

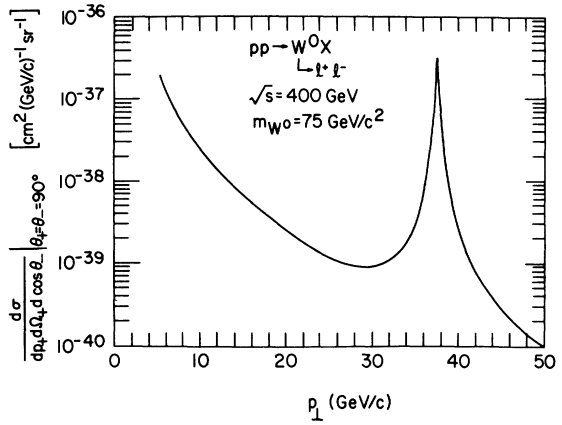

FIG. 19. $d\sigma/dp_+d\Omega_+d\cos\theta_-$ at $\theta_+=\theta_-=90°$ vs $p_\perp$ for l^+, l^- both from W^0 and γ_V with $m_{W^0}\approx 75$ GeV/c^2, at $\sqrt{s}=400$ GeV, pp reaction.

and $\sqrt{s}=400$ GeV. The general shape of the distribution consists of two peaks due to the W propagator, coming from W^0's moving forward and backward in the center-of-mass system. At $p_\perp=\frac{1}{2}m_W$, the W^0 must be at rest and the two peaks coalesce into a single broader peak. (See the discussion of double jets in Sec. V.)

V. HIGH-p HADRONS

In this section we estimate the cross section for producing high-$p_\perp$ hadrons at very high energies, with emphasis on the energy of the proposed ISABELLE accelerator. There are several reasons for doing this: (a) One is interested in the expected range of $p_\perp$ that will be experimentally detectable for pure hadronic studies; (b) estimates of backgrounds for W search coming from hadronic processes are needed; (c) estimates of hadronic jets coming from the W decays are needed.

In order to make these estimates we use the

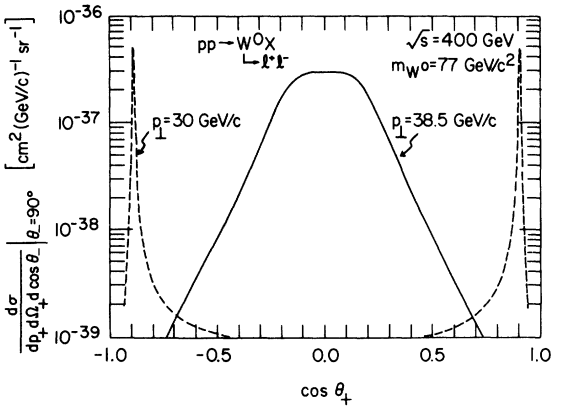

FIG. 20. $d\sigma/dp_+d\Omega_+d\cos\theta_-|_{\theta_-=90°}$ vs $\cos\theta_+$ for various $p_\perp$ values.

quark-parton model with the structure functions used in the earlier sections of this paper. The basic process will be taken as quark-quark (or antiquark) scattering, and solely for the purpose of giving a range of estimates we will use as representative the standard massless-gluon exchange,[28] giving $p_\perp^{-4}$ behavior, and the Field and Feynman[29] parametrization, giving $p_\perp^{-8}$.

The cross sections we will present will be for hadronic jets, i.e., quark partons. The cross section for π's depends on the distribution function $G(x)/x$, $x = p_\pi/p_j$, which gives the differential distribution of the number of π's of momentum p_π coming from a jet of momentum p_j,[28] especially on its behavior near $x = 1$. Since we are interested only in estimates and since $G(x)$ is not well known, we will not attempt to do a refined job of calculating the ratio of the π cross section to the jet cross section. Rather we will follow Bjorken's rough estimates[30] based on $G(x) \approx \frac{2}{3}(1-x)$; for a more detailed consideration see Field and Feynman[29] or Ellis, Jacob, and Landshoff.[31] For the Field-Feynman model, $\sigma(\pi)/\sigma(\text{jet}) \approx 10^{-2}$ over the range $10\ \text{GeV}/c < p_\perp < 50\ \text{GeV}/c$ at $\sqrt{s} = 400$ GeV; for the gluon model $\sigma(\pi)/\sigma(\text{jet})$ varies from $\frac{1}{15}$ at $p_\perp = 10$ GeV/c to about $\frac{1}{40}$ at $p_\perp = 50$ GeV/c at $\sqrt{s} = 400$ GeV. We will come back to the question of π's from W decays.

In the vector-gluon model, once the structure functions are given, all that is needed is the effective gluon coupling α_{eff}. We assume a single neutral-gluon coupling independent of flavor. In order to determine its value, we require the calculated cross section to be smaller than the cross section measured at the ISR at the highest $p_\perp$ measurement. In the curves shown in Fig. 21, we use $\alpha_{\text{eff}} = 0.05$. This gives $Ed\sigma/d^3p$ for π's to be about 3×10^{-36} cm^2/GeV^2 sr at $\sqrt{s} = 53$ GeV and $p_\perp = 9$ GeV/c. The experimental value from the CCR experiment is also about 3×10^{-36} cm^2/GeV^2 sr. It is of interest to compare this with the effective gluon coupling one would obtain from quantum chromodynamics. If we assume that it arises from eight colored gluons A_i^μ coupling via $\frac{1}{2}g\bar{q}\lambda_i\gamma_\mu q A_i^\mu$, the averaging on initial colors and summing on final colors gives

$$\alpha_{\text{eff}}^2 = \left(\frac{g^2}{4\pi}\right)^2 (\tfrac{1}{2})^4 \tfrac{1}{9} \sum_{i,j} [\text{Tr}(\lambda_i\lambda_j)]^2 = \frac{2}{9}\left(\frac{g^2}{4\pi}\right)^2$$

or

$$\alpha_{\text{eff}} = \frac{\sqrt{2}}{3}\frac{g^2}{4\pi}. \tag{5.1}$$

Although it is not at all certain that asymptotic freedom can be used here, let us see what it says for the coupling constant. According to asymptotic freedom[33] the coupling constant depends on momentum according to

$$\frac{g^2(q^2)}{4\pi} = \frac{g^2(M^2)/4\pi}{1 + (25/12\pi)[g^2(M^2)/4\pi]\ln(q^2/M^2)}, \tag{5.2}$$

and $g^2(M^2)/4\pi \approx \frac{1}{2}$ for $M^2 = 1$. A pion of momentum 9 GeV/c comes on the average from a jet of momentum 12 GeV/c in this model with these structure functions. If we identify $q^2 = 2p_{\text{jet}}^2$, then $g^2/4\pi$ evaluated at $q^2 = 288$ GeV^2 is, according to Eq. (5.2),

$$\frac{g^2}{4\pi} = 0.17,$$

or

$$\alpha_{\text{eff}} = 0.08.$$

This coupling gives a cross section a factor 2.6 higher than those we use.

In Fig. 21 we show the cross section $d\sigma/dpd\Omega$ for a jet produced at 90° and $\sqrt{s} = 400$ GeV as given by the vector-gluon model and by the Field-Feynman quark-quark cross section (but our structure functions). Because the mother-daughter relation differs for $p_\perp^{-4}$ and $p_\perp^{-8}$, the cross sections for π production intersect at about $p_\perp = 9$ GeV/c, where they both are about 10^{-33} cm^2 (GeV/c)$^{-1}$ sr^{-1} (for π's). The Field-Feynman curve for π's agrees to within about a factor of 2 with extrapolation of the CCR fit to $\sqrt{s} = 400$ GeV. That fit to the inclusive cross section for π^0's at 90° is[32]

$$E\frac{d\sigma}{dp^3} = \frac{1.54\times10^{-26}}{(p_\perp)^{8.24}}\, e^{-26.1p_\perp/\sqrt{s}}\ (\text{cm}^2/\text{GeV}^2\ \text{sr}). \tag{5.3}$$

At $p_\perp = 35$ GeV/c, relevant for the background of

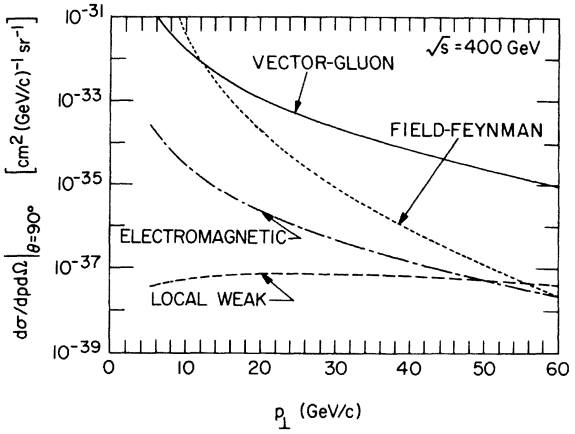

FIG. 21. Predicted cross sections $d\sigma/dpd\Omega$ for hadronic jets at 90° as a function of $p_\perp$ for various models.

a W of mass 70 GeV/c^2, the cross section for π's is about

$$\frac{d\sigma}{dpd\Omega} \approx \begin{cases} 4\times10^{-36}\ \text{cm}^2/\text{GeV}, & \text{for the gluon model,} \\ 3\times10^{-38}\ \text{cm}^2/\text{GeV}, & \text{for the Field-Feynman model.} \end{cases}$$

For comparison, we also show the electromagnetic and pure weak cross sections vs $p_\perp$ at 90° and $\sqrt{s}=400$ GeV. For pure weak we use a point coupling with Fermi strength for charge-changing coupling. If the gluon theory is a good estimate we will not be able to expose these weak and electromagnetic contributions. The Field-Feynman cross section for the π's intersects the electromagnetic near 35 GeV/c. The cross section there is quite small, $d\sigma/dpd\Omega \approx 10^{-38}$ cm^2/GeV for π's.

Figure 22 shows how the cross section in the gluon model depends on energy. The curves shown correspond to $\sqrt{s}=2000$, 800, 400, and 100 GeV. At $p_\perp=20$ GeV/c, the gain from 400 GeV to highest energy is about a factor of 3 while at $p_\perp=50$ GeV/c it is about a factor of 5. The Field-Feynman model gives similar results. Just as for the gluon, the weak and electromagnetic cross sections have very slow increase with energy and so the situation does not change much at higher energies; the intersection will move to slightly smaller $p_\perp$ and the cross section at intersection will increase a small amount. The conversion of jets into pions has been calculated for the weak and electromagnetic interactions by Craig.[34]

We have also calculated the same cross sections for $\bar{p}p$. The difference is very small for $p_\perp < 50$ GeV/c, and is shown in Fig. 23. Thus $\bar{p}p$ backgrounds will not be very different from pp. It would be of fundamental interest to measure this difference, but it will probably be very difficult.

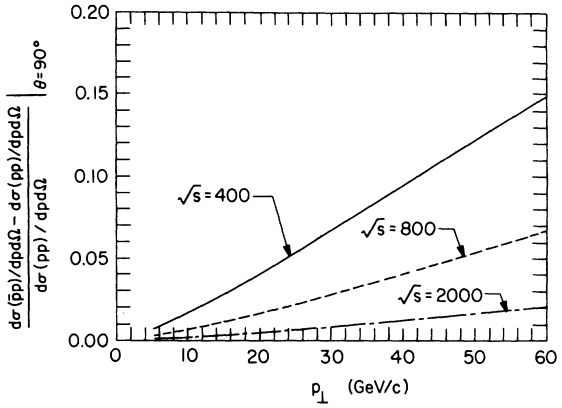

FIG. 23. Comparison of pp and $\bar{p}p$ cross sections for hadronic jets at 90° from the vector-gluon model. The numbers for $\sqrt{s}$ are in units of GeV.

It is of some interest to see what the jet distributions look like at other angles. The change is very slow with angle. Figure 24 shows the $p_\perp^{-4}$ distributions out to 50 GeV/c for $\theta=90°$, 20°, 6°. The shape of the falloff is very sensitive to the distribution functions near $x=1$ and would give a good measure of them if the very small cross sections could be measured.

Turning to the problem of backgrounds for leptonic W decay, there seem to be three types to consider: (a) too many particles jamming the counters, (b) high-$p_\perp$ hadrons faking leptons, (c) real leptons not associated with the W. We leave it to the experimentalists to use our estimates to deal with problems (a) and (b). For problem (c) we use the empirical relation[27] that e/π or μ/π is about 10^{-4} over a wide range of conditions and assume it will be true in this very high $p_\perp$ realm as well. The hadronic background shown in Fig. 6 in

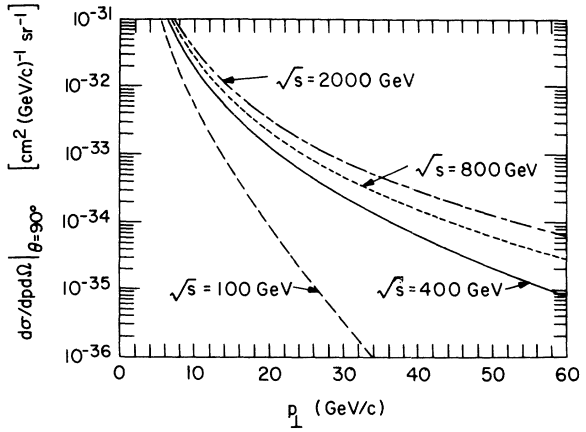

FIG. 22. Predicted cross sections for hadronic jets at 90° from the vector-gluon model at various center-of-mass energies.

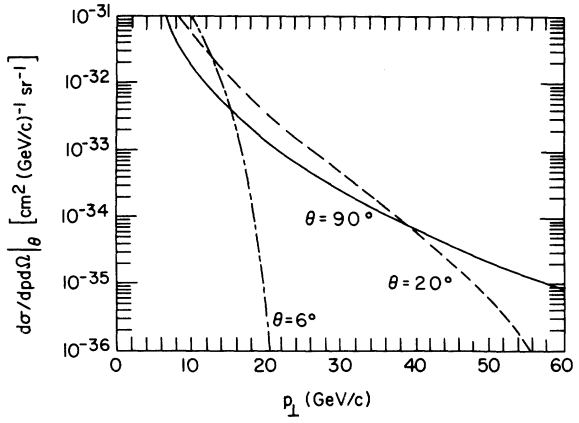

FIG. 24. Predicted cross section for hadronic jets at various angles and $\sqrt{s}=400$ GeV from the vector-gluon model.

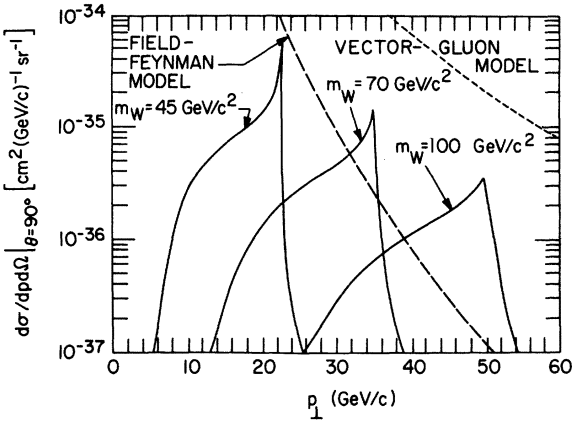

FIG. 25. Predicted cross sections for hadronic jets at 90°, $\sqrt{s}=400$ GeV from W^+ and W^- of various masses. Vector-gluon and Feynman-Field model backgrounds are shown.

Sec. IV was obtained by folding the distribution function $G(x)$ into the gluon jet cross section and multiplying by 10^{-4}. (Thus, the π distribution can be read off that figure by multiplying by 10^4.) Evidently, the Field-Feynman hadronic background will be far below the gluon background and is not shown.

It would be very interesting if hadronic decays of W mesons could be studied. Figure 25 shows the cross section for producing hadron jets at 90°, $\sqrt{s}=400$ GeV, through a $W^{\pm}$. All quantum numbers are summed on because it will probably prove very difficult to determine the quantum numbers of a jet. See Eq. (B15) in Appendix B. This curve is essentially similar to that for W decay leptons except that the background is now hadronic jets. The $p_\perp^{-4}$ and $p_\perp^{-8}$ backgrounds are shown on the same figure. From these curves we see that it is not certain that the W can be detected through its hadronic jets in spite of the fact that its branching ratio into hadrons is much larger than that into leptons.

There is an additional point: Hadronic decays of the W will probably have to be jet studies because the hadrons coming from the jet will not show the characteristic peaking. The peaking of the jet distribution is washed out in the hadron distribution. This can be easily seen from the relation[35]

$$E\frac{d\sigma}{d^3p}\bigg|_\pi = \frac{1}{p}\int dp_j G\left(\frac{p}{p_j}\right) E\frac{d\sigma}{d^3p_j}\bigg|_{\text{jet}}. \qquad (5.4)$$

Because $Ed\sigma/d^3p_j$ is sharply peaked,

$$E\frac{d\sigma}{d^3p}\bigg|_\pi \propto G\left(\frac{2p}{m_W}\right), \qquad (5.5)$$

and the characteristic peaking is lost.

We wish to look briefly at the question of double jets. These are very directly related to the elementary cross section for parton-parton interactions and the structure functions, as pointed out by Bjorken[30]; there are no integrals and so these measurements could give very valuable information about these quantities. In Figs. 26(a) and 26(b) we show the distribution in angle of a recoiling jet when one jet is detected at 90° for various $p_\perp$, according to the vector-gluon model or the Field-Feynman model. (Again, we are using not only the Field-Feynman cross section but our structure functions as well. We also take no account of small transverse momentum of the quarks. Field *et al.* have included this in a forthcoming study[36] and say it can have significant effects.) These are not presented here as definitive tests of the models but merely to give an estimate of the size of the cross sections and rates of variation. The behavior near the ends where the cross section falls rapidly measures the behavior of the structure function near $x=1$. Otherwise the behavior is rather smooth. It is probably worth commenting that, although the Field-Feynman cross section is more peripheral ($\sim 1/\hat{s}\hat{t}^3$) than the vector gluon

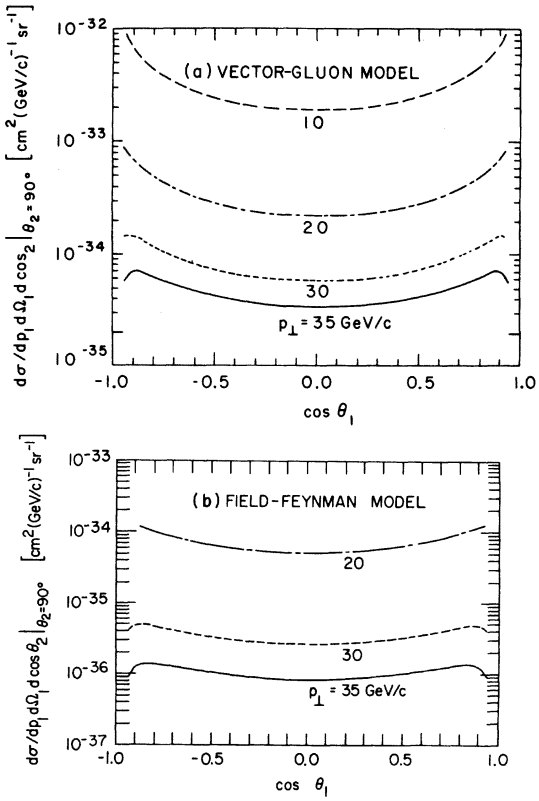

FIG. 26. Double-jet cross sections $d\sigma/dp_1 d\Omega_1 d\cos\theta_2|_{\theta_2=90°}$ as a function of $\cos\theta_1$, the angle of the second jet for various values of $p_\perp$ (a) vector-gluon model, (b) Feynman-Field model.

($\sim 1/\hat{t}^2$), this does not show up clearly when plotted in the usual way, as we have done in Fig. 26. One might expect the Field-Feynman model to give more peaking at small angles, rather than less than the vector-gluon model. The reason it does not is that as θ gets small, for fixed $p_\perp$, the energy of the parton-parton collision $(s)^{1/2}$ grows and compensates for $\hat{t}$ getting smaller [see Eq. (5.6)]. The main reason the curves are so slowly varying over most of the range is that $\hat{s}$ and $\hat{t}$ are slowly varying with $\cos\theta$ over a wide range of $\cos\theta$ [see Eq. A(12)].

The structure of double jets coming from the W is much more interesting. From $p_\perp = m_W/2$, a broad smooth bump at 90° is seen. As $p_\perp$ is reduced, however, the recoil peak moves off 90° (symmetrically) and becomes much sharper. See Fig. 27. The reason for this is that the energy $\hat{s} \approx m_W^2$ at which the parton-parton collisions takes place is related to the angle θ of the second jet by

$$\hat{s} = 2p_\perp^2\left(1 + \frac{1}{|\sin\theta|}\right), \tag{5.6}$$

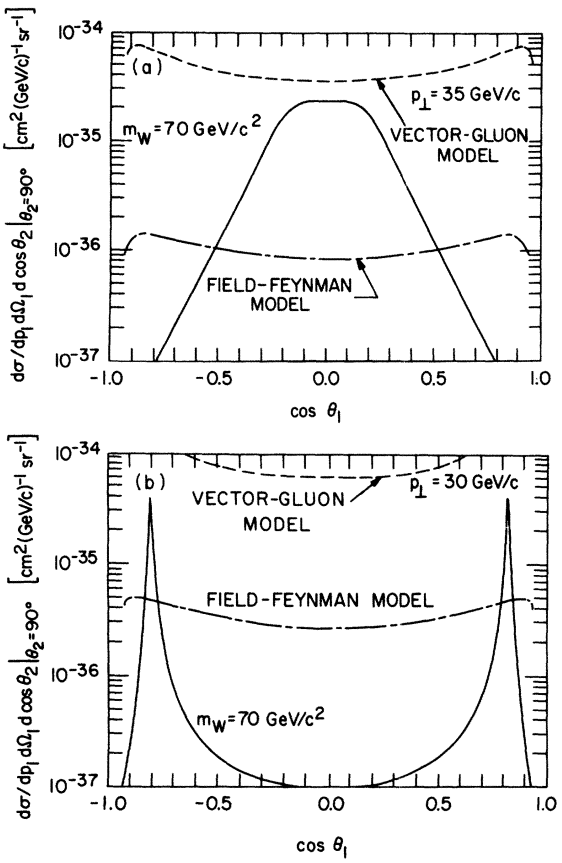

FIG. 27. Double-jet cross section $d\sigma/dp_1 d\Omega_1 d\cos\theta_2|_{\theta_2=90°}$ as a function of $\cos\theta_1$. The peaked curve shows jets from W decay, $m_W = 70$ GeV/c^2. The vector-gluon and Feynman-Field backgrounds are also shown. (a) $p_\perp = 35$ GeV/c, (b) $p_\perp = 30$ GeV/c.

or a fixed $p_\perp$

$$d\cos\theta = \frac{|\tan\theta|\,\sin^2\theta}{2p_\perp^2}\,d\hat{s}$$

$$\approx \frac{\Gamma m_W}{p_\perp^2}\,|\tan\theta|\,\sin^2\theta\,.$$

The W peak in $\hat{s}$ occurs at

$$|\sin\theta| = \frac{1}{[(m_W^2/2p_\perp^2) - 1]}; \tag{5.7}$$

for $p_\perp$ smaller than m_W this angle becomes small and the width in $\cos\theta$ becomes small. Of course, at the same time the cross section becomes smaller and the background becomes larger and whether or not this sharper peak will stand out above the background is not certain. The momentum resolution possible for jet measurements will have an important bearing on this. We simply point this out as an interesting possibility.

The double-jet cross section as a function of $p_\perp$ for fixed angle will have a sharp peak, as does the double-lepton distribution in Fig. 19. The height of this peak relative to the background can be read off Fig. 27(a).

VI. TRANSVERSE-MOMENTUM SMEARING

All calculations in the earlier parts of this paper assume that the W is produced with no transverse momentum. Obviously, this is not exactly true and the peaking of the lepton spectrum will be smeared to some extent by the W's transverse motion. The question is: How much? In order to answer this we need two things, an estimate of the W's transverse momentum and a way of incorporating the transverse motion into our calculations.

For the second point, since we are interested in estimates we will not attempt to incorporate transverse motion of the quarks into the parton model, but will assume that the model gives the longitudinal motion of the W correctly and will put the transverse motion in by hand. This is not completely consistent but should not cause any trouble if $\vec{K}_\perp$ of the W is not too large. This technique was previously used by Halzen,[37] but we disagree with some of his conclusions.

The main reason we concern ourselves with this point is that experiment indicates that as more massive objects are produced, their average transverse momentum increases as well. Thus we must expect that the W can carry considerably more than 300 MeV/c of transverse momentum. It has been found that a reasonable fit to production of a particle of mass M has the cross section[38]

$$E\frac{d\sigma}{d^3K} \propto \exp[-b(\vec{K}_\perp^2 + M^2)^{1/2}], \tag{6.1}$$

with $b \approx 6$ (GeV/c)$^{-1}$. The root-mean-square momentum in a transverse direction for this distribution is

$$(\langle K_x^2\rangle)^{1/2} = \left(\frac{M}{b}\right)^{1/2}. \tag{6.2}$$

For $b = 6$ (GeV/c)$^{-1}$, this gives

$$(\langle K_x^2\rangle)^{1/2} = \begin{cases} 2.58 \text{ GeV}/c & \text{for } M = 40 \text{ GeV}/c^2, \\ 3.42 \text{ GeV}/c & \text{for } M = 70 \text{ GeV}/c^2, \\ 4.08 \text{ GeV}/c & \text{for } M = 100 \text{ GeV}/c^2. \end{cases}$$

These are very large momenta, but much smaller than the W mass, in fact very slightly larger than the W width so, as we shall see, a dramatic effect is not expected. Given these numbers, we can see no good reason to fear that the transverse-momentum smearing will wash out the signal, in contrast to Halzen's conclusion.[37] The parameter that he chooses to show the W peak completely washed out corresponds to a transverse momentum of nearly 200 GeV/c for the W.

We assume that the W is produced with longitudinal momentum given by the formulas in the Appendix. We simply add to it a transverse momentum $K_\perp$ with the distribution (6.1). The modification of the kinematics due to $K_\perp$ is taken into account by noting that a lepton of momentum p coming from the decay of an off-mass-shell W of mass $(\hat{s})^{1/2}$ and momentum K satisfies

$$p \cdot K = \tfrac{1}{2}\hat{s}. \tag{6.3}$$

The modification to the arguments of the structure functions is insignificant, since it is of order $K_\perp^2/s$. For simplicity, we neglect the alignment of the W and assume that it decays isotropically. We will also neglect $K_\perp^2$ with respect to $\hat{s}$ and work to terms linear in $K_\perp$. Then the only modification of our formula is that the Jacobian in (A14) is modified:

$$\frac{2p_\perp}{(1-4p_\perp^2/\hat{s})^{1/2}} \to \frac{2p_\perp - K_x}{(1-4p_\perp^2/\hat{s}+4p_\perp K_x/\hat{s})^{1/2}} \tag{6.4}$$

(where $p_\perp$ is in the x direction) and the lower limit in (A15) is changed from $4p_\perp^2$ to $4p_\perp^2 - 4p_\perp K_x$.

The result of numerically integrating this approximate expression is shown in Fig. 28. We see that the sharp peaking at $m_W/2$ is lost, but that the general shape of the W signal remains and is still far above the estimated backgrounds.

It is easy to estimate the size of the smearing effect analytically. First of all, it is clear that on the lower side of the peak, as soon as

$$1 - \frac{4p_\perp^2}{M^2} > \frac{4p_\perp}{M}\langle K_x^2\rangle^{1/2}$$

the effect of smearing will be unimportant. For

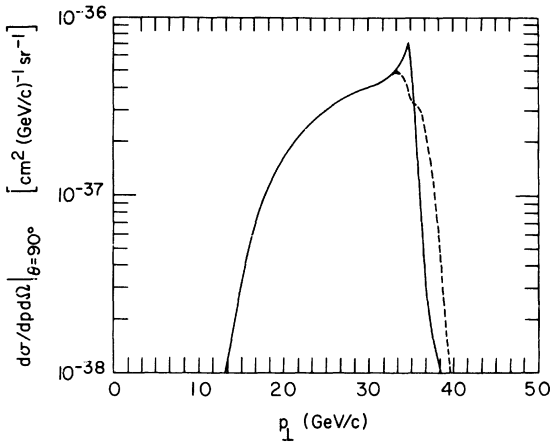

FIG. 28. Effect of the W transverse-momentum distribution $\exp[-6(K_\perp^2 + m_W^2)^{1/2}]$; solid line from Fig. 6, dotted line, after smearing.

$M = 70$ GeV/c^2 and $b = 6$ (GeV/c)$^{-1}$, this occurs for $p_\perp \approx 30$ GeV/c. For $p_\perp$ at or above the peak at $m_W/2$ the events come primarily from W's with very small longitudinal momentum so the effect of smearing can be obtained by evaluating the $\hat{s}$ integral over the W peak, keeping only the rapidly varying Jacobian square root. This integral is readily evaluated:

$$\int_{4p_\perp^2 - 4p_\perp K_x}^{\infty} d\hat{s}\, \frac{1}{(\hat{s}-m_W^2)^2 + 4m_W^2\Gamma^2}\, \frac{1}{(\hat{s}-4p_\perp^2+4p_\perp K_x)^{1/2}} = \frac{\pi}{m_W\Gamma}\, \frac{\cos\varphi/2}{[(m_W^2 - 4p_\perp^2 + 4p_\perp K_x)^2 + 4m_W^2\Gamma^2]^{1/4}}, \tag{6.5}$$

where

$$\cos\varphi = \frac{m_W^2 - 4p_\perp^2 + 4p_\perp K_x}{[(m_W^2 - 4p_\perp^2 + 4p_\perp K_x)^2 + 4m_W^2\Gamma^2]^{1/2}} \tag{6.6}$$

Let $R(K_x)$ denote the ratio of this integral for $K_x \gg \Gamma$ to the value when $K_x = 0$. Then

$$R(K_x) = \left(\frac{2\Gamma}{K_x}\right)^{1/2}. \tag{6.7}$$

For $\Gamma \approx 0.5$ GeV and $K_x = 3.5$ GeV this reduction is about 0.4, which agrees roughly with the numerical integrations. This formula shows that the reduction factor decreases slowly with K_x; another factor of 2 reduction would require $(\langle K_x^2\rangle)^{1/2} \approx 14$ GeV/c.

The behavior above the peak can be readily seen from Eq. (6.5): The effect of K_x is to shift $m^2 \to m^2 + 4p_\perp K_x$. The upper edge of the sharp peak in the unsmeared case comes at $p_\perp = m/2$. Using the shifted value of M, this corresponds to $K_x = p_\perp - m^2/4p_\perp$. Thus, substituting in (6.1), we expect a behavior proportional to

$$\exp\left[-b\left(p_\perp+\frac{m_W^2}{4p_\perp}\right)\right],$$

which is a good representation of the numerical calculations.

We conclude that it is unlikely, on the basis of our present best estimates, that the transverse momentum of the W will damage the beautiful lepton spectrum very much.

VII. CONCLUDING REMARKS

(1) The lepton-pair-production data are consistent with the Drell-Yan model, using quark and antiquark structure functions with color, and a steep x variation near $x=1$ for the sea quarks, $\propto(1-x)^7$.

(2) The total W production cross sections are about 10^{-34}–10^{-33} cm^2 for $s/m_W{}^2>10$ and do not increase very much as $s/m_W{}^2$ increases. Though the W production cross sections are more than one order of magnitude higher in $\bar{p}p$ reactions than in pp reactions in the $s/m_W{}^2<10$ region, the ratio decreases rapidly as $s/m_W{}^2\geq 10$.

(3) The production of W's is concentrated in the small x_F region. It spreads out as $s/m_W{}^2$ decreases.

(4) The distributions of single leptons from the W decay have a characteristic peak at $p_\perp=\frac{1}{2}m_W$. The height of the peak decreases as $s/m_W{}^2$ decreases, or as the W width increases, or as the lepton direction moves away from 90°. It is well above the lepton background from electromagnetic production at $\sqrt{s}=400$ GeV, for a wide range of W masses ≥ 10 GeV/c^2.

(5) The lepton cross section from weak interactions with an infinitely heavy W^+ crosses that from the electromagnetic interaction at $p_\perp\approx 25$ GeV/c, $\sqrt{s}=400$ GeV.

(6) Once the weak production dominates the electromagnetic production, the parity violation of the weak interaction gives characteristically different distributions for leptons and antileptons. This is a striking consequence of the quark-parton model. Its observation would give direct support to this model. This provides a handle for detecting the presence of weak interactions and distinguishing various weak-interaction models. This parity-violation effect is even more striking in the $\bar{p}p$ reactions.

(7) The cross sections for single-hadron and hadron-jet production via strong interactions in the quark-parton model are quite sensitive to the large $p_\perp$ dependence of the elementary cross sections. Behaviors of $p_\perp{}^{-4}$ and $p_\perp{}^{-8}$ give substantially different results at ISABELLE energies.

(8) Hadronic-jet decays of the W should be plentiful. However, the direct hadronic background may well be too high to allow this mode of detecting the W. The best chance is in double-jet experiments where a sharp peak in $p_\perp$ dependence is expected. For observations of single hadrons the sharp peak is expected to be washed out.

(9) Transverse motions of the W, neglected in the quark-parton model, will have the effect of reducing the sharpness of the upper edge of the W peak in the $p_\perp$ distributions of single leptons, but should still leave the signal well above the background.

Thus all indications are that the long-awaited intermediate bosons are within the reach of the next generation of colliding-beam machines.

ACKNOWLEDGMENTS

We have had useful discussions with many colleagues, especially J. D. Bjorken, M. Creutz, R. D. Field, T. Gaisser, F. Halzen, L. Lederman, L. Okun', R. Palmer, F. Paige, E. Paschos, C. Quigg, N. P. Samios, and D. Sivers.

APPENDIX A: GENERAL FORMULATION

The calculations in the body of the paper are of cross sections for the double inclusive process

$$h+h'\to p+p'+X, \tag{A1}$$

where h and h' are hadrons and p, p' are leptons or "jets" of hadrons. This process, based upon the original hypothesis of Ref. 12, is assumed to proceed through the mechanism indicated in Fig. 29, in which h emits a massless quark q, h' emits a massless quark q', and q collides with q' to form p and p' through the two-body reaction

$$q+q'\to p+p'. \tag{A2}$$

The main kinematic assumption of the model is that the quark q carries a fraction x of the three-momentum of h ($0\leq x\leq 1$). We choose the direction of relative motion of h and h' as the z axis, or longitudinal direction, with h defined as moving in the $+z$ direction, and work in the frame where the motion of h and h' is purely longitudinal.

We adopt the notational convention that a particle

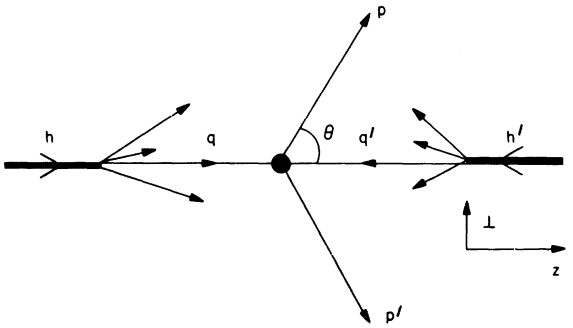

FIG. 29. Kinematics of quark-parton model.

p has four-momentum $p_\mu \equiv (p_0, p_x, p_y, p_z)$ and define

$$\begin{aligned} p_\perp &\equiv (p_x^2 + p_y^2)^{1/2}, \\ p &\equiv (p_\perp^2 + p_z^2)^{1/2}, \\ \mu_p &= (p_0^2 - p^2)^{1/2}, \\ \theta_p &= \arccos(p_z/p), \\ \phi_p &= \arccos(p_x/p_\perp), \\ y_p &= \operatorname{arccosh}[p_0/(p_\perp^2 + \mu_p^2)^{1/2}]. \end{aligned} \tag{A3}$$

The total squared invariant energy of the system is

$$s = (h_\mu + h'_\mu)^2 . \tag{A4}$$

We will be interested in large s and throughout this appendix make the assumption that the masses of h, h', p, p' can be neglected in comparison with $\sqrt{s}$. We therefore set them equal to zero, throughout:

$$\mu_h = \mu_{h'} = \mu_p = \mu_{p'} = \mu_q = \mu_{q'} = 0 . \tag{A5}$$

Thus we can write the explicit forms of the four-momenta q, q'

$$\begin{aligned} q_\mu &\equiv (xh, 0, 0, xh), \\ q'_\mu &= (x'h', 0, 0, -x'h'). \end{aligned} \tag{A6}$$

Each observed particle has in principle three kinematic degrees of freedom. The fixed transverse momenta in (A6) introduce two constraints so that there remain four kinematic degrees of freedom for the reaction (A1) in this model. One of these four may be taken to represent a trivial azimuthal rotation about the z axis, leaving three nontrivial degrees of freedom. It is convenient to choose the following three invariant quantities to specify the reaction:

$$\begin{aligned} \hat{s} &= Q_\mu^2 , \\ \hat{t} &= (p_\mu - q_\mu)^2 , \\ \hat{y} &= y_Q - y_H , \end{aligned} \tag{A7}$$

where

$$\begin{aligned} Q_\mu &= q_\mu + q'_\mu , \\ H_\mu &= h_\mu + h'_\mu . \end{aligned}$$

Other kinematical variables can be expressed in terms of these three. In particular:

$$x = e^{\hat{y}}(\hat{s}/s)^{1/2}, \quad x' = e^{-\hat{y}}(\hat{s}/s)^{1/2} . \tag{A8}$$

Thus the differential cross section $(d^3\sigma/d\hat{s}d\hat{t}d\hat{y})$ can be factorized as follows:

$$\begin{aligned} \frac{d\sigma}{d\hat{s}d\hat{t}d\hat{y}} &= \sum_{q,q'} \frac{d\sigma_{qq'}(\hat{s},\hat{t})}{d\hat{t}} \frac{dN_{qq'}}{d\hat{s}d\hat{y}} \\ &= \sum_{q,q'} \frac{d\sigma_{qq'}(\hat{s},\hat{t})}{d\hat{t}} \frac{dN_{qq'}}{sdxdx'} . \end{aligned} \tag{A9}$$

Here $d\sigma_{qq'}/d\hat{t}$ is the differential cross section for the elementary process (A2); q and q' label the different types of quark that can contribute and $(dN_{qq'}/dxdx')$ represents the joint probability density to find a parton of type q having momentum fraction x in h, together with a parton of type q' having momentum fraction x' in h'. For any other choice of three variables u_1, u_2, u_3 we can simply transform variables and write

$$\frac{d\sigma}{du_1 du_2 du_3} = J(u_1u_2u_3) \sum_{q,q'} \frac{d\sigma_{qq'}}{dt} \frac{dN_{qq'}}{sdxdx'} , \tag{A10}$$

where

$$J(u_1u_2u_3) = \left| \frac{\partial(\hat{s},\hat{t},\hat{y})}{\partial(u_1u_2u_3)} \right|$$

is the Jacobian, and $\hat{s}, \hat{t}, \hat{y}$ (and thence x and x') are expressed in terms of u_1, u_2, u_3. Double or single differential cross sections or total cross sections can be obtained by integrating (A10) over appropriate regions.

The problem of calculating cross sections thus separates into three parts:

(i) the choice of variables $u_1u_2u_3$ relevant to the problem in question, and the calculation of the Jacobian together with any necessary integration limits,

(ii) the calculation of the relevent cross section $d\sigma_{qq'}/d\hat{t}$,

(iii) the calculation of the "structure function" $dN_{qq'}/dxdx'$.

We continue here with a discussion of the kinematic factors, and discuss the choice of variables appropriate for two-particle, single-particle, and total cross sections. We always choose to plot those cross sections which most directly relate momentum and angular acceptances to counting rates.

Two-particle distributions. These are the simplest to discuss, though not to measure. In the model we consider here there is no net transverse motion of the pp' system so only one independent transverse momentum remains. The desired cross section is

$$\frac{d\sigma}{dpd\Omega\, d\cos\theta'} = \frac{1}{2\pi \sin\theta \sin^2\theta'} J(p_\perp, y_p, y'_p) \times \sum_{qq'} \frac{d\sigma(\hat{s},\hat{t})}{d\hat{t}} \frac{dN_{qq'}}{sdxdx'} . \tag{A11}$$

Working in the hadron-hadron center-of-mass system, we have

$$
\begin{aligned}
&J(p_\perp, y_p, y_{p'}) = \frac{\partial(\hat{s}, \hat{t}, \hat{y})}{\partial(p_\perp, y_p, y_{p'})} = 2p_\perp \hat{s}\,,\\
&\hat{s} = 4p_\perp^2 \cosh^2 \hat{y}_p\,,\\
&\hat{y}_p = \tfrac{1}{2}(y_p - y_{p'})\,,\\
&\hat{t} = -p_\perp^2[1+\exp(-2\hat{y}_p)]\,,\\
&\hat{y} = \tfrac{1}{2}(y_p + y_{p'})\,,
\end{aligned}
\tag{A12}
$$

and x, x' are given by Eq. (A8).

Single-particle distributions. These involve a single integration. The cross section of interest is $p_0 d\sigma/dp_\perp dp_z$, which is the invariant cross section integrated over the azimuth. The convenient variables to use in this case are $(\hat{s}, p_\perp, y_p)$, and the desired cross sections are obtained by integrating over $\hat{s}$. These can be related to the standard variables by introducing $\hat{y}_p$, the rapidity of particle p in the center-of-mass system of the elementary process:

$$
\begin{aligned}
&\hat{y} = y_p - \hat{y}_p\,,\\
&\frac{(\hat{s})^{1/2}}{2} = p_\perp \cosh \hat{y}_p\,,\\
&\hat{t} = -\tfrac{1}{2}\hat{s}(1-\cos\hat{\theta}_p)\\
&\quad = -\tfrac{1}{2}\hat{s}(1-\tanh\hat{y}_p)\,,
\end{aligned}
\tag{A13}
$$

(where the last two relations make use of the assumption of zero mass for p). The Jacobian is then

$$
J(\hat{s}, p_\perp, y_p) \equiv \frac{\partial(\hat{y}, \hat{t})}{\partial(p_\perp, y_p)} = \frac{2p_\perp}{(1-4p_\perp^2/\hat{s})^{1/2}}\,. \tag{A14}
$$

Using Eq. (A10) we obtain the cross section plotted in the figures

$$
\begin{aligned}
\frac{d\sigma}{dp d\Omega} &= \frac{p_\perp}{\sin\theta} p_0 \frac{d\sigma}{d^3p}\\
&= \frac{1}{\sin\theta}\frac{d\sigma}{dp_\perp dy_p d\varphi}\\
&= \frac{1}{2\pi}\int d\hat{s}\,\frac{d\sigma}{d\hat{s}\,dp_\perp dy_p}\\
&= \int \frac{2p_\perp}{(1-4p_\perp^2/\hat{s})^{1/2}}\,\frac{d\sigma}{d\hat{s}\,d\hat{t}\,d\hat{y}}\,d\hat{s}\,.
\end{aligned}
\tag{A15}
$$

Note that the second equation of (A13) has two solutions, $y_p = \pm|y_p|$ whose contributions must be added. The integration limits are given by the constraints

$$
\begin{aligned}
&4p_\perp^2 \le \hat{s} \le s\,,\\
&0 \le x \le 1\,,\\
&0 \le x' \le 1\,.
\end{aligned}
\tag{A16}
$$

Using (A8), (A12), and (A16) the latter two can be rearranged to yield

$$
\exp(\pm 2\hat{y}_p) \le \left[\frac{\sqrt{s}}{p_\perp}\exp(\pm y_p) - 1\right] \equiv A_\pm\,,
$$

which is equivalent to

$$
-\tfrac{1}{2}\ln(A_\mp) \le |\hat{y}_{p_1}| \le \tfrac{1}{2}\ln(A_\pm)\,. \tag{A17}
$$

By definition $|y_p|$ is positive, so if we define

$$
\tilde{Y}_\pm = \max[0, -\tfrac{1}{2}\ln A_\mp]\,, \tag{A18}
$$

then the limits on $\hat{s}$ may be obtained, using (A13),

$$
4p_\perp^2 \cosh^2 \tilde{Y}_\pm \le \hat{s} \le \min[s, 4p_\perp^2 \cosh^2(\tfrac{1}{2}\ln A_\pm)]\,. \tag{A19}
$$

Distribution of the pp'-diparticle system. Here the individual momenta of p or p' are not measured but only their sum. In this case only the $\hat{t}$ integrated cross section of Eq. (A9) is of interest:

$$
\frac{d\sigma}{d\hat{s}\,d\hat{y}} = \sum_{qq'} \sigma_{qq'}(\hat{s})\frac{dN_{qq'}}{s\,dx\,dx'}\,, \tag{A20}
$$

where

$$
\sigma_{qq'}(\hat{s}) = \int_{-s}^{0} d\hat{t}\,\frac{d\sigma_{qq'}}{d\hat{t}}(\hat{s}, \hat{t})\,. \tag{A21}
$$

Equivalently Eq. (A20) can be written as

$$
\frac{d\sigma}{dx\,dx'} = \sum_{qq'} \sigma_{qq'}(sxx')\frac{dN_{qq'}}{dx\,dx'}\,. \tag{A22}
$$

In most cases we are interested in the distribution in $\hat{s}$ and x_F, where $x_F = (p_z^* + p_z'^*)/\tfrac{1}{2}\sqrt{s} = x - x'$,

$$
\frac{d\sigma}{d\hat{s}} = \sum_{qq'} \sigma_{qq'}(\hat{s})\int_0^1\int_0^1 \frac{dN_{qq'}}{dx\,dx'}\,\delta(sxx' - \hat{s})\,dx\,dx' \tag{A23}
$$

and

$$
\frac{d\sigma}{d\hat{s}\,dx_F} = \sum_{qq'} \sigma_{qq'}(\hat{s})\,\frac{1}{(x_F^2 + 4\tau)^{1/2}}\,\frac{dN_{qq'}}{s\,dx\,dx'}\,, \tag{A24}
$$

with the constraints

$$
\begin{aligned}
&x = \tfrac{1}{2}[(x_F^2 + 4\hat{s}/s)^{1/2} + x_F]\,,\\
&x' = \tfrac{1}{2}[(x_F + 4\hat{s}/s)^{1/2} - x_F]\,.
\end{aligned}
$$

In the text we use m^2 in place of $\hat{s}$ to be consistent with the more usual notation.

The structure functions. As we mentioned earlier $dN_{qq'}/dx\,dx'$ is the probability of finding a parton q in hadron h with momentum xh and a parton q' in hadron h' with $x'h$. So it is a product of two probability functions:

$$
\frac{dN_{qq'}}{dx\,dx'} = \frac{q(x)}{3}\,\frac{q'(x')}{3}\,, \tag{A25}
$$

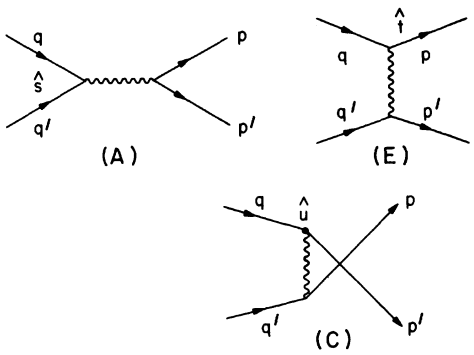

FIG. 30. Vector-exchange mechanisms.

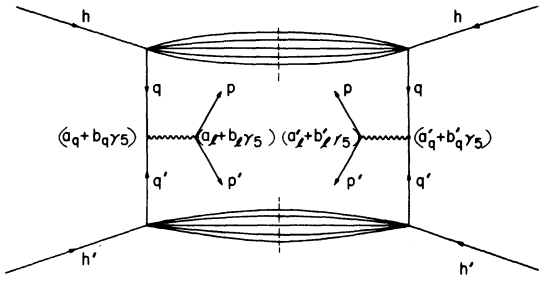

FIG. 31. General structure of V,A couplings.

where $q(x)$, $q(x')$ are the functions defined in Eqs. (2.1) and (2.2). In the three-color four-quark models, q, q' can be u, $\bar{u}$, d, $\bar{d}$, s, $\bar{s}$, and c, $\bar{c}$. We assume that there are negligible amounts of charmed quark in the proton and equal amounts of all other quarks in the sea as given in Eq. (2.2). These probability functions are also measured in ep inelastic scattering. The probability functions are related to the structure function

$$\nu W_2 = x\{\tfrac{4}{9}[u(x)+\bar{u}(x)]+\tfrac{1}{9}[d(x)+\bar{d}(x)] + \tfrac{1}{9}[s(x)+\bar{s}(x)]\}. \quad \text{(A26)}$$

The factors in front of the probability functions are squared quark charges. Notice that here u includes the two valence u quarks of the proton and the u quark from sea. The explicit forms of the quark probability functions are given in Eq. (2.1). The probability functions of partons in the antiproton are

$$\bar{u}_{\bar{p}} = u_p, \quad \bar{d}_{\bar{p}} = d_p, \quad \text{(A27)}$$

and those in the antiproton sea are the same as in the proton.

APPENDIX B: FORMULAS FOR VARIOUS PROCESSES

From Appendix A we see that to give the various p, p' distributions, basically we need two ingredients. The elementary cross sections of $qq' \to pp'$ and the probability functions of q, q' in the hadrons h, h'. The interactions of $qq' \to pp'$ considered here are point interactions via a spin-one field (except in the Field-Feynman model). There are three types of interactions annihilation (A), exchange (E), and crossed exchange (C), as shown in Fig. 30, or, in other words, poles in the $\hat{s}$, $\hat{t}$, and $\hat{u}$ channels. In the following we shall list all the formulas for the various processes we discussed in the text. Cross sections are given in units of GeV^{-2}.

Electromagnetic processes

Here the mediating particle is the photon γ_V. It is a pure vector interaction.

(a) $q\bar{q}$ annihilation to lepton pair $l\bar{l}$. The differential cross section is

$$\frac{d\sigma^A}{d\hat{t}} = \frac{1}{8\pi\hat{s}^2}\frac{e_q^2(4\pi\alpha)^2}{\hat{s}^2}(\hat{t}^2+\hat{u}^2), \quad \text{(B1)}$$

where $\alpha = \frac{1}{137}$, and e_q^2 is the charge of quark q in units of $(4\pi\alpha)^{1/2}$, $\hat{t} \equiv (q-p)^2$, $\hat{u} = (q-p')^2$ [see Fig. 29]. The $\hat{t}$ integrated cross section is

$$\sigma^A(\hat{s}) = \frac{\hat{s}}{12\pi}\frac{e_q^2(4\pi\alpha)^2}{\hat{s}^2}. \quad \text{(B2)}$$

Together with the structure functions, using Eq. (B1), Eq. (A9), and Eq. (A25), we obtain

$$\frac{d\sigma}{d\hat{s}\,d\hat{t}\,d\hat{y}} = \frac{1}{s}\sum_{q=u,d,s}\tfrac{1}{3}[q(x)\bar{q}(x')+\bar{q}(x)q(x')] \times e_q^2\frac{2\pi\alpha^2}{\hat{s}^4}(\hat{t}^2+\hat{u}^2). \quad \text{(B3)}$$

Using Eqs. (B2), (A23), and (A24) we obtain

$$\frac{d\sigma}{d\hat{s}} = \sum_{q=u,d,s}\frac{\hat{s}}{12\pi}\left(\frac{4\pi\alpha}{\hat{s}}\right)^2 e_q^2\int_0^1\int_0^1 dx\,dx'\,\delta(sxx'-\hat{s})\tfrac{1}{3}[q(x)\bar{q}(x')+\bar{q}(x)q(x')] \quad \text{(B4)}$$

and

$$\frac{d\sigma}{d\hat{s}\,dx_F} = \sum_{q=u,d,s}\frac{\hat{s}}{12\pi}\left(\frac{4\pi\alpha}{\hat{s}}\right)^2 e_q^2\frac{1}{s(x_F^2+4\tau)^{1/2}}\tfrac{1}{3}[q(x)\bar{q}(x')+\bar{q}(x)q(x')]. \quad \text{(B5)}$$

Notice that with $\hat{s}=m^2$, Eq. (B5) gives Eq. (2.3), which is written in the more conventional form.

(*b*) *Electromagnetic jet production.* The process involved here is $qq'\to pp'$ via γ_V exchanges in all three $\hat{s}$, $\hat{t}$, $\hat{u}$ channels.

$$\frac{d\sigma}{d\hat{s}d\hat{t}d\hat{y}}=\frac{2}{s}\sum_q[q(x)\bar{q}(x')+\bar{q}(x)q(x')]\frac{1}{8\pi\hat{s}^2}\frac{e_q^2\sum_p e_p^2(4\pi\alpha)^2}{\hat{s}^2}(\hat{t}^2+\hat{u}^2)$$
$$+\frac{1}{s}\sum_q[q(x)+\bar{q}(x)]\sum_{q'}[q'(x')+\bar{q}'(x')]\frac{1}{8\pi\hat{s}^2}e_q^2e_{q'}^2(4\pi\alpha)^2\left[\frac{(\hat{s}^2+\hat{u}^2)}{\hat{t}^2}+\frac{(\hat{t}^2+\hat{s}^2)}{\hat{u}^2}\right]. \tag{B6}$$

Here q, q' are summed over u, d, s. The sum over p in addition includes the charmed quark. The $(\hat{t}^2+\hat{u}^2)$ term comes from the annihilation process; the $(\hat{s}^2+\hat{u}^2)$ term comes from the t-channel exchange and the $(\hat{t}^2+\hat{s}^2)$ term comes from the u-channel exchange. Both quark and antiquark jets are summed on.

Weak-interaction processes

For these processes only the annihilation graph (A) of Fig. (30) is relevant, since W exchange is forbidden for lepton production and negligible for jets.

(*a*) *Production of* W^+ ($\to\mu^+\nu_\mu$ *or* $e^+\nu_e$). Here the interaction via W^+ is $V-A$. The differential cross sections for $q\bar{q}\to W^+\to l\bar{l}$ are

$$\frac{d\sigma^{A,\pm}}{d\hat{t}}=\frac{1}{8\pi\hat{s}^2}\frac{4(G/\sqrt{2})^2m_W^4\eta_c}{(\hat{s}-m_W^2)^2+4m_W^2\Gamma^2}(\hat{t}^2\pm\hat{u}^2), \tag{B7}$$

where $G=10^{-5}/m_p^2$, $\Gamma=8(1/12\pi)(G/\sqrt{2})m_W^3$, the $W^\pm$ full width as given in Eq. (4.2) and explained in Sec. IV A; $q\bar{q}$ stands for all quark-antiquark pairs with charge one and $l\bar{l}$ stands for $\mu^+\nu_\mu$ or $e^+\nu_e$. For $q\bar{q}=u\bar{d}$, $\eta_c=\cos^2\theta_C$ (where θ_C is the Cabibbo angle), and for $q\bar{q}=u\bar{s}$, $\eta_c=\sin^2\theta_C$. The "+" in Eq. (B7) corresponds to the pure vector and pure axial-vector parts of the interaction. The "-" in Eq. (B7) corresponds to vector–axial-vector interference. The $\hat{t}$-integrated cross section is

$$\sigma^{A,+}(\hat{s})=\frac{\hat{s}}{12\pi}\frac{4(G/\sqrt{2})^2m_W^4\eta_c}{(\hat{s}-m_W^2)^2+4m_W\Gamma^2} \tag{B8}$$

Notice that $\sigma^{A,-}(\hat{s})=0$.

Again using Eqs. (B7) and (A9), we obtain

$$\frac{d^3\sigma}{d\hat{s}d\hat{t}d\hat{y}}=\frac{1}{s}\sum_{\epsilon=\pm}\{\tfrac{1}{3}[u(x)\bar{d}(x')+\epsilon\bar{d}(x)u(x')]\cos^2\theta_C+\tfrac{1}{3}[u(x)\bar{s}(x')+\epsilon\bar{s}(x)u(x')]\sin^2\theta_C\}$$
$$\times\frac{1}{8\pi\hat{s}^2}\frac{4(G/\sqrt{2})^2m_W^4}{(\hat{s}-m_W^2)^2+4m_W^2\Gamma^2}(\hat{t}^2+\epsilon\hat{u}^2). \tag{B9}$$

(For distributions of $\mu^+\nu_\mu$ produced weakly without a W^+, we can simply set $m_W\to\infty$ and $\Gamma=0$.) Using (B8), (A23), and (A24) we obtain

$$\frac{d\sigma}{d\hat{s}}=\frac{\hat{s}}{12\pi}\frac{4(G/\sqrt{2})^2m_W^4}{(\hat{s}-m_W^2)^2+4m_W^2\Gamma^2}\int_0^1\int_0^1 dxdx'\,\delta(sxx'-\hat{s})\tfrac{1}{3}[u(x)\bar{d}(x')+\bar{d}(x)u(x')]. \tag{B10}$$

We have combined the $\cos^2\theta_C$ and $\sin^2\theta_C$ term because the sea quarks are all the same in our calculation. To obtain the total production cross section for W^+, which then decays to $\mu^+\nu_\mu$, we use

$$\int\frac{d\hat{s}f(\hat{s})}{(\hat{s}-m_W^2)^2+4m_W^2\Gamma^2}\approx\frac{\pi}{2m_W\Gamma}f(m_W^2). \tag{B11}$$

Thus we get

$$\sigma_{W^+\to\mu^+\nu_\mu}=\tfrac{1}{8}2\pi(G/\sqrt{2})m_W^2\int_0^1\int_0^1 dxdx'\,\delta(sxx'-m_W^2)\tfrac{1}{3}[u(x)\bar{d}(x')+\bar{d}(x)u(x')]. \tag{B12}$$

As discussed in Sec. IV A, the branching ratio of $W^+\to\mu^+\nu_\mu$ is $\frac{1}{8}$, so

$$\sigma_{W^+}=8\sigma_{W^+\to\mu^+\nu_\mu}. \tag{B13}$$

Similarly to (B5), we can derive $d\sigma/d\hat{s}dx_F$ for the W^+. Integrating over $\hat{s}$ and multiplying by 8, we obtain the x_F distribution for the W^+,

$$\frac{d\sigma_{W^+}}{dx_F} = 2\pi(G/\sqrt{2})\,\frac{1}{(x_F{}^2 + 4m_W{}^2/s)^{1/2}}\,\tfrac{1}{3}[u(x)\bar{d}(x') + \bar{d}(x)u(x')]\,, \tag{B14}$$

where x and x' are the same as specified for Eq. (A24).

(*b*) *Production of* W^- ($\to \mu^-\bar{\nu}_\mu$ or $e^-\bar{\nu}_e$). Equations (B10)–(B14) for the W^+ all apply except for replacing the quark structure functions $u\bar{d}$ by $d\bar{u}$, respectively, and the use of the approximation $\theta_C = 0$.

(*c*) *Production of jets from* $W^\pm$ *decay*. For each specific quark-antiquark decay mode of the W there will be an expression such as those in (a) and (b) above. Since, however, the nature of the individual quark is not observed, we must combine all the terms. This leads to three changes:

(1) Adding outgoing quark and antiquark symmetrizes (B9) in $\hat{t}^2$ and $\hat{u}^2$.
(2) Adding W^+ and W^- symmetrizes in $u\bar{d}$ and $d\bar{u}$.
(3) There are six decay channels for each $W^\pm$ ($u\bar{d}$ and $c\bar{s}$ for each of three colors).

The result for zero Cabibbo angle is

$$\frac{d\sigma}{d\hat{s}\,d\hat{t}\,d\hat{y}} = \frac{1}{s}\,[u(x)\bar{d}(x') + \bar{d}(x)u(x') + \bar{u}(x)d(x') + d(x)\bar{u}(x')]\,\frac{4}{8\pi\hat{s}^2}\,\frac{4(G/\sqrt{2})^2 m_W{}^4}{(s - m_W{}^2)^2 + 4\Gamma^2 m_W{}^2}\,(\hat{t}^2 + \hat{u}^2)\,. \tag{B15}$$

If we wish to consider the local limit, we can no longer neglect the exchange graphs (*C*) and (*E*) in Fig. (30) since all three propagators approach unity in the infinite-mass limit. The angular distributions also become identical, but the color counting and association of the right structure functions require consideration of all three. Since the interest in this case is as a lower limit we ignore the neutral-current contribution to charm production and the s component of the proton. These approximations should not underestimate the cross sections by more than about a factor of 2. The formula used is

$$\frac{d\sigma}{d\hat{s}\,d\hat{t}\,d\hat{y}} = \frac{G^2}{2\pi}\,\frac{1}{s}\left(\left\{\sum_{q=u,\,d}[q(x) + \bar{q}(x)]\right\}\left\{\sum_{q=u,\,d}[q(x') + \bar{q}(x')] - \sum_{\substack{q=u,\,d\\ \bar{u},\,\bar{d}}} q(x)q(x')\right\}\right)\frac{\hat{t}^2 + \hat{u}^2}{\hat{s}^2}\,. \tag{B16}$$

(*d*) *Production of* W^0 ($\to e^+e^-$ *or* $\mu^+\mu^-$). Here the coupling is still vector and axial vector. However, their strength is very model dependent. A further complication is that there are inference terms with γ_ν. We shall calculate the general $(a + b\gamma_5)\gamma_\mu$ couplings for the Drell-Yan model as shown in Fig. 31.

The differential cross sections for $q\bar{q} \to l\bar{l}$ are

$$\frac{d\sigma^{A,\pm}}{d\hat{t}} = \frac{1}{8\pi\hat{s}^2}\,\frac{\beta^{A,\pm}}{\Delta}\,(\hat{t} \pm \hat{u})\,, \tag{B17}$$

where

$$\beta^{A,\pm} = g^2 g'^2 (a_q a'_q + b_q b'_q)(a_l a'_l + b_l b'_l)\,,$$

and

$$\begin{aligned} &\beta^{A,-} = g^2 g'^2 (a_q b'_q + a'_q b_q)(a_l b'_l + a'_l b_l)\,, \\ &\Delta = (\hat{s} - m_{W^0}{}^2)^2 + 4m_{W^0}{}^2(\Gamma^0)^2\,. \end{aligned} \tag{B18}$$

For a pure W^0 term, in the SU(2) ⊗ U(1) model of Weinberg and Salam,

$$\begin{aligned} &g^2 = g'^2 = (G/\sqrt{2})m_{W^0}{}^2\,, \\ &a'_i = a_i = \sqrt{2}\,(I_z - 2e_i \sin^2\theta_W)\,, \quad b'_i = b_i = \sqrt{2}\,I_z\,, \\ &m_{W^0} = 76/\sin 2\theta_W\ (\mathrm{GeV}/c^2)\,, \end{aligned} \tag{B19}$$

where I_z is the z component of the isospin of the particle i, e_i is the charge of particle i in units of $(4\pi\alpha)^{1/2}$, and θ_W is the Weinberg angle. For the quarks and leptons we consider here that the values of a's and b's are

$$\begin{aligned} &a_u = a_c = (1 - \tfrac{8}{3}\sin^2\theta_W)/\sqrt{2}\,, \quad b_u = b_c = 1/\sqrt{2}\,, \\ &a_s = a_d = -(1 - \tfrac{4}{3}\sin^2\theta_W)/\sqrt{2}\,, \quad b_s = b_d = -1/\sqrt{2}\,, \\ &a_\mu = a_e = -(1 - 4\sin^2\theta_W)/\sqrt{2}\,, \quad b_\mu = b_e = -1/\sqrt{2}\,, \\ &a_\nu = b_\nu = 1/\sqrt{2}\,, \text{ for both } \nu_\mu \text{ and } \nu_e\,. \end{aligned} \tag{B20}$$

Given these couplings the W^0 full width can be calculated to be

$$\Gamma^0 = (2A_\nu + 2A_e + 3A_c + 3A_d + 3A_u + 3A_s)\frac{1}{2}\frac{1}{12\pi}\frac{G}{\sqrt{2}}\, m_{W^0}{}^3 , \tag{B21}$$

where $A_i \equiv (a_i{}^2 + b_i{}^2)$. The factor in front of A_i is the number of channels with the same coupling strength. Now the leptonic branching ratio, say the $\mu\bar{\mu}$ channel, is

$$B^0_{l\bar{l}} = \Gamma^0_{l\bar{l}}/\Gamma^0 = \frac{A_e}{2A_\nu + 2A_e + 3A_c + 3A_d + 3A_u + 3A_s} . \tag{B22}$$

Using the formulas here and Eqs. (A9) and (B5), we obtain

$$\frac{d\sigma^A}{d\hat{s}\,d\hat{t}\,d\hat{y}} = \frac{1}{s}\sum_{\epsilon=\pm}\sum_{q=u,d,s}\tfrac{1}{3}[q(x)\bar{q}(x') + \epsilon\bar{q}(x)q(x')]\frac{1}{8\pi\hat{s}^2}\frac{A_q A_l (G/\sqrt{2})^2 m_{W^0}{}^4}{(\hat{s}-m_{W^0}{}^2)^2 + 4m_{W^0}{}^2(\Gamma^0)^2}(\hat{t}^2 + \epsilon\hat{u}^2) . \tag{B23}$$

Similar to Eq. (B10) $d\sigma/d\hat{s}$ and σ_{W^0} can also be calculated. We only list σ_{W^0},

$$\sigma_{W^0} = \pi(G/\sqrt{2})m_{W^0}{}^2\int_0^1\int_0^1 dx\,dx'\,\delta(sxx' - m_{W^0}{}^2)\sum_{q=u,d,s}\tfrac{1}{3}[q(x)\bar{q}(x') + \bar{q}(x)q(x')]A_q . \tag{B24}$$

For the W^0 and γ_V interference term,

$$g^2 = 4\pi\alpha e_q{}^2 , \quad g'^2 = (G/\sqrt{2})m_{W^0}{}^2 , \tag{B25}$$

$$a'_i = 1 , \quad b_i = 0 ,$$

$$a'_i = \sqrt{2}(I_z - 2e_i \sin^2\theta_W) , \quad b'_i = \sqrt{2}\, I_z . \tag{B26}$$

Thus the β's in Eq. (B18) can be calculated according to Eqs. (B25) and (B26). The propagator factor in Eq. (B17) becomes

$$\frac{1}{\Delta} = \mathrm{Re}\left(\frac{1}{\hat{s}}\frac{1}{\hat{s} - m_{W^0}{}^2 - i2m_{W^0}\Gamma^0}\right) = \frac{1}{\hat{s}}\frac{\hat{s} - m_{W^0}{}^2}{(\hat{s}-m_{W^0}{}^2)^2 + 4m_{W^0}{}^2(\Gamma^0)^2} . \tag{B27}$$

Using these equations we can calculate all the formulas as before.

Gluon processes

The production of hadronic jets by vector-gluon interactions is closely analogous to the electromagnetic jet production discussed earlier. The propagator is the same, and the coupling constant is α_S instead of α (the value of α_S is discussed in the text). Otherwise the main difference comes in the color analysis. Unlike the photon which is a color singlet, there exists an octet of vector gluons with SU(3)-invariant couplings to the quarks. Carrying out the appropriate SU(3) counting we are led to

$$\frac{d\sigma}{d\hat{s}\,d\hat{t}\,d\hat{y}} = \frac{8}{s}\sum_q [q(x)\bar{q}(x') + \bar{q}(x)q(x')]\frac{1}{8\pi\hat{s}^2}\frac{(4\pi\alpha_s)^2}{\hat{s}^2}(\hat{t}^2 + \hat{u}^2)$$
$$+\frac{1}{s}\sum_q [q(x) + \bar{q}(x)]\sum_{q'}[q'(x') + \bar{q}'(x')]\frac{1}{8\pi\hat{s}^2}(4\pi\alpha_s)^2\left(\frac{\hat{s}^2+\hat{t}^2}{\hat{u}^2} + \frac{\hat{s}^2+\hat{u}^2}{\hat{t}^2}\right), \tag{B28}$$

where the sums over q, q' run over u, d, s.

Field-Feynman quark-scattering model

According to Field and Feynman[29] the elementary cross section for quark-quark scattering, averaged over all quark final states, is

$$\frac{d\sigma}{d\hat{t}} = \frac{2300}{0.3894}\frac{1}{\hat{s}(-\hat{t})^3}\ (\mathrm{GeV}^{-4}) , \tag{B29}$$

where $\hat{s}$ and $\hat{t}$ are in units of GeV^2. Since the two resulting jets are indistinguishable we must symmetrize between $\hat{t}$ and $\hat{u}$, and obtain

$$\frac{d\sigma}{d\hat{s}\,d\hat{t}\,d\hat{y}} = \frac{1}{s}\sum_q [q(x) + \bar{q}(x)]\sum_{q'}[q'(x') + \bar{q}'(x')]\left[\frac{1}{(-\hat{t})^3} + \frac{1}{(-\hat{u})^3}\right]\frac{2300}{0.3894\hat{s}}\ (\mathrm{GeV}^{-6}) , \tag{B30}$$

where, as usual, q, q' are summed over u, d, s.

*Work supported by U. S. Energy Research and Development Administration.

[1]H. Yukawa, Proc. Phys. Math. Soc. Japan 17, 48 (1935). The modern version of the intermediate boson was discussed in T. D. Lee, C. N. Yang, and M. Rosenbluth, Phys. Rev. 75, 905 (1949); M. Gell-Mann, Rev. Mod. Phys. 31, 834 (1959); T. D. Lee and C. N. Yang, Phys. Rev. Lett. 4, 307 (1960).

[2]T. D. Lee, Phys. Rev. Lett. 26, 801 (1971).

[3]S. Weinberg, Phys. Rev. Lett. 19, 1264 (1967); A. Salam, in *Elementary Particle Theory: Relativistic Groups and Analyticity (Nobel Symposium No. 8)*, edited by N. Svartholm (Almqvist and Wiksell, Stockholm, 1968), p. 367. For a review see E. S. Abers and B. W. Lee, Phys. Rep. 9C, No. 1 (1973).

[4]F. J. Hasert *et al.*, Phys. Lett. 46B, 138 (1973); B. Aubert *et al.*, Phys. Rev. Lett. 32, 1454 (1974); 32, 1457 (1974); B. C. Barish *et al.*, *ibid.* 34, 538 (1975). For a review see H. Williams, in *Particles and Fields '76*, proceedings of the Annual Meeting of the Division of Particles and Fields of the American Physical Society, Brookhaven National Laboratory, 1976, edited by H. Gordon and R. E. Peierls (BNL, Upton, New York, 1977), p. D95.

[5]D. P. Sidhu, Phys. Rev. D 14, 2235 (1976); C. Albright, C. Quigg, J. Smith, and R. Shrock, *ibid.* 14, 1780 (1976); R. M. Barnett, *ibid.* 14, 2990 (1976); V. Barger and D. V. Nanopoulos, Wisconsin Report No. COO-562, 1976 (unpublished). For recent reviews on the subject, see J. J. Sakurai, in Proceedings of the International Conference on Neutrino Physics, Aachen, Germany, 1976 (unpublished); R. M. Barnett, in *Particles and Fields '76* (Ref. 4), p. D77.

[6]L. B. Okun', Yad. Fiz. 3, 590 (1966) [Sov. J. Nucl. Phys. 3, 426 (1966)]; Y. Yamaguchi, Nuovo Cimento 43, 193 (1966); L. M. Lederman and B. G. Pope, Phys. Rev. Lett. 27, 765 (1971).

[7]R. L. Jaffe and J. R. Primack, Nucl. Phys. B61, 317 (1973); Yu. A. Golubkov, A. A. Ivanilov, Yu. P. Nikitin, and G. V. Kohnov, Yad. Fiz. 18, 393 (1973) [Sov. J. Nucl. Phys. 18, 203 (1974)]; R. W. Brown, K. O. Mikaelian, and M. K. Gaillard, Nucl. Phys. B75, 112 (1974).

[8]R. B. Palmer, E. A. Paschos, N. P. Samios, and L. L. Wang, Phys. Rev. D 14, 118 (1976).

[9]L. B. Okun' and M. B. Voloshin, ITEP report, Moscow, 1976 (unpublished); L. B. Okun', ITEP report, Moscow, 1976 (unpublished). C. Quigg, Rev. Mod. Phys. 49, 297 (1977).

[10]R. Cutler and D. Sivers, Phys. Rev. D 16, 679 (1977).

[11]S. Gershstein and J. Zeldovich. Zh. Eksp. Teor. Fiz. 35, 821 (1958) [Sov. Phys.—JETP 8, 570 (1959)]; R. Feynman and M. Gell-Mann, Phys. Rev. 109, 193 (1958); Y. K. Lee, L. W. Mo, and C.-S. Wu, Phys. Rev. Lett. 10, 253 (1963). For a recent critical discussion of the experimental status of CVC see F. P. Calaprice and B. R. Holstein, Nucl. Phys. A273, 523 (1976).

[12]We use specifically the Drell-Yan model. S. D. Drell and T.-M. Yan, Phys. Rev. Lett. 25, 316 (1970) and Ann. Phys. (N.Y.) 66, 578 (1971); J. Kuti and V. Weisskopf, Phys. Rev. D 4, 3418 (1971); P. V. Landshoff and J. C. Polkinghorne, Nucl. Phys. B33, 221 (1971); B36, 643 (1972); S. M. Berman, J. D. Bjorken, and J. B. Kogut, Phys. Rev. D 4, 3388 (1971); J. Pakvasa, D. Parashar, and S. F. Tuan, *ibid.* 10, 2124 (1974); 11, 214 (1975); G. Farrar, Nucl. Phys. B77, 429 (1974); V. Barger and R. J. N. Phillips, *ibid.* B73, 269 (1974); H. P. Paar and E. A. Paschos, Phys. Rev. D 10, 1502 (1974) and G. Altarelli *et al.*, Nucl. Phys. B92, 413 (1975).

[13]D. C. Hom *et al.*, Phys. Rev. Lett. 37, 1374 (1976).

[14]D. C. Hom *et al.*, Phys. Rev. Lett. 36, 1236 (1976).

[15]L. Kluberg *et al.*, Phys. Rev. Lett. 37, 1451 (1976).

[16]M. Binkley *et al.*, Phys. Rev. Lett. 37, 571 (1976).

[17]K. S. Anderson *et al.*, Princeton report, 1976 (unpublished).

[18]Notice that the valence-quark distributions we use here are the ones from S. Pakvasa *et al.*, in Ref. 12. Owing to the change in the exponent of $(1-x)$ for the sea quark, we also change the coefficient so that it still gives a good fit to *ep* inelastic scattering in the $x \lesssim 0.1$ region where the sea contributions dominate. Recently other forms of valence distributions were found to fit the data better [see (a) below]; and also other forms of the parton-quark model have been developed for *pp* scattering [see (b) below]. Until these refinements are well understood to the level of accuracy needed in our analysis, we use the conventional approach. (a) R. E. Taylor, in *High Energy Physics*, Proceedings of the European Physical Society International Conference, Palermo, 1975, edited by A. Zichichi (Editrice Compositori, Bologna, 1976), p. 377; in *Proceedings of the 1975 International Symposium on Lepton and Photon Interactions at High Energies, Stanford, California*, edited by W. T. Kirk (SLAC, Stanford, 1976), p. 679. (a) A. Donnachie and P. V. Landshoff, Nucl. Phys. B112, 233 (1976).

[19]J. H. Christenson *et al.*, Phys. Lett. 25, 1523 (1970).

[20]S. Brodsky and G. Farrar, Phys. Rev. Lett. 31, 1153 (1975); V. A. Matveev, R. M. Muradyan, and A. N. Tavkhelidze, Lett. Nuovo Cimento 7, 719 (1973).

[21]L. M. Lederman and B. G. Pope, Phys. Lett. 66B, 486 (1977).

[22]There are indications both theoretically [see (a) below] and experimentally [see (b) below] that scaling may break down badly in the extremely small x region (say $x \lesssim 0.02$). If so, the calculations done here have to be revised. (a) V. N. Gribov, Zh. Eksp. Teor. Fiz. 57, 1306 (1970) [Sov. Phys.—JETP 30, 709 (1970)]; A. De Rújula, H. Georgi, and H. D. Politzer, Ann. Phys. (N.Y.) 103, 315 (1977). (b) H. L. Anderson *et al.*, Chicago, Harvard, Illinois, and Oxford report, 1976 (unpublished).

[23]This dip was first noticed by G. Farrar in Ref. 12.

[24]S. Glashow, J. Iliopoulos, and L. Maiani, Phys. Rev. D 2, 1285 (1970).

[25]See Eqs. (B7) and (B9) in Appendix B for details and the Cabibbo-angle dependence of the coupling.

[26]E. G. Cazzoli *et al.*, Phys. Rev. Lett. 34, 1125 (1975); G. Goldhaber *et al.*, *ibid.* 37, 255 (1976); B. Knapp *et al.*, *ibid.* 37, 882 (1976).

[27]J. P. Boymond *et al.*, Phys. Rev. Lett. 33, 112 (1974); J. A. Appel *et al.*, *ibid.* 33, 722 (1974); F. W. Büsser *et al.*, CERN report, 1976 (unpublished); V. V. Abramov *et al.*, Phys. Lett 64B, 365 (1976); E. W. Beier *et al.*, Phys. Rev. Lett. 37, 1117 (1976); L. Baum *et al.*, Phys. Lett. 60B, 485 (1976); A. Staude and F. Muller (private communication); K. Winter, Phys. Lett. 57B, 479 (1975); A. Browman, Phys. Rev. Lett. 37, 246 (1976). See also L. N. Leder-

man, in *Proceedings of the 1975 International Symposium on Lepton and Photon Interactions at High Energies, Stanford, California* [Ref. 18(a)], p. 265; in *Particles and Fields '76* (Ref. 4), p. A31.
[28]S. M. Berman, J. D. Bjorken, and J. B. Kogut, Phys. Rev. D 4, 3388 (1971).
[29]R. D. Field and R. P. Feynman, Phys. Rev. D 15, 2590 (1977).
[30]J. D. Bjorken, Phys. Rev. D 8, 4098 (1973).
[31]J. Ellis, M. Jacob, and P. Landshoff, Nucl. Phys. B108, 93 (1976).
[32]F. W. Büsser *et al.*, Phys. Lett. 46B, 471 (1973).
[33]H. D. Politzer, Phys. Rev. Lett. 26, 1346 (1973); D. Gross and F. Wilczek, *ibid.* 26, 1343 (1973); A. De Rujula, H. Georgi, and S. Glashow, Phys. Rev. D 12, 147 (1975).
[34]K. H. Craig, Nucl. Phys. B109, 156 (1976).
[35]J. D. Bjorken, Acta Phys. Polon. B5, 893 (1974).
[36]R. D. Field, G. C. Fox, and R. P. Feynman (unpublished). We thank Dr. Field for telling us about these results.
[37]F. Halzen, Phys. Rev. D 15, 1929 (1977).
[38]L. Lederman, report to APS/DPF 1976 Brookhaven meeting (unpublished); M. Chen in *Particle Searches and Discoveries—1976*, proceedings of the 2nd International Conference in High Energy Physics at Vanderbilt University, edited by R. S. Panvini (AIP, New York, 1976); F. Halzen, in Proceedings of the VIIth International Colloquium on Multiparticle Reactions, Tutzing, Germany, 1976 (unpublished).